Chapter 1

A brief review of high-energy nuclear collisions

1.1 Introduction

The characteristics of all elementary particles and the interactions experienced by them, are described by a unified, renormalizable gauge field theory, called the standard model (SM). The SM however, explains only three fundamental interactions namely the strong, the electromagnetic and the weak, out of the four that exist in nature. So far a similar renormalizable quantum theory for the fourth fundamental interaction, the gravitation, could not be developed. Quarks and leptons, the basic constituents of matter, participate in one or more of these interactions. High-energy heavy-ion interaction deals mainly with the bulk properties of hadronic/partonic matter, where the properties of these fundamental interactions are coupled with the macroscopic matter aspects of nuclear physics. For example, quantum chromodynamics (QCD), the non-abelian gauge theory of strong interaction, predicts that at high pressure and/or high temperature, the usual nuclear matter may undergo a transition to a color conducting deconfined state of quasi-free quarks and gluons called the quark-gluon plasma (QGP), and the QGP then makes a transition to a state of color neutral hadrons [1, 2]. In a strongly interacting extended QCD state phase transitions like these are not only a topic of interest, but they may also help us answer some of the basic questions that are related to the evolution of the universe after its birth, as well as to some astrophysical phenomena still taking place within it. It is speculated that

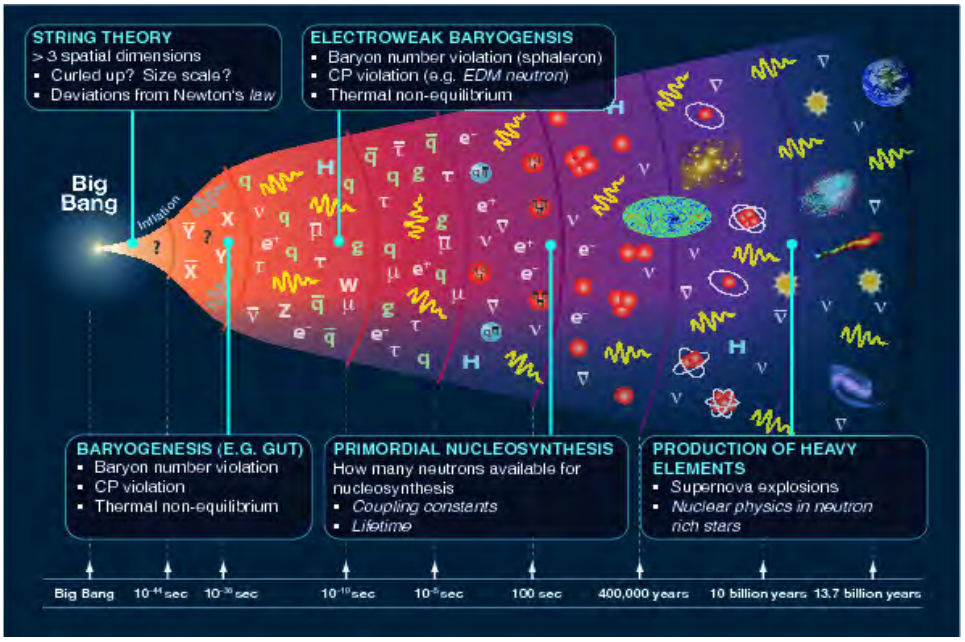

Figure 1.1: A schematic of the time history of the universe [3].

the early universe passed through a QGP $\rightarrow$ hadron phase transition within the first few microseconds of its birth, popularly known as the big bang. In this respect high-energy heavy-ion interaction relates the science of small, i.e. the physics of elementary particles, to the science of large, the cosmology. Using the properties of QGP one can explore and test the predictions of QCD in its natural scale (Λ_{qcd}). In Figure 1.1 we show a schematic of the time (or equivalently the temperature) history of the universe. It is also speculated that shortly after the big bang, as the baby universe expanded and cooled down, it passed through several symmetry breaking processes that lead to different types of phase transitions. One such transition is associated with the electroweak symmetry breaking process that provides masses to the elementary particles. This transition took place at a temperature $T \gtrsim 200$ GeV. It is also related to the electroweak baryon number violating process that leads to the baryon-antibaryon abundance asymmetry observed in nature. Another transition from the QGP $\rightarrow$ hadronic phase of matter took place at $T \lesssim 200$ MeV. This was due to the spontaneous breaking of chiral symmetry of the $SU_c(3)$ color group. Lattice QCD calculations suggest that both these transitions may not be accompanied at all with any kind of discontinuity in the temperature dependence of the free energy and/or its derivative(s). They are rather smooth cross-overs from one state to the other [4–7]. Lattice simulations also suggest that at vanishing baryochemical potential both the phase transitions might have taken place essentially at the same point. After hadronization, when the universe was just several seconds old, nucleosynthesis started. Gradually the radiation dominated universe turned into a matter dominated phase. After about 10 μsec of the big bang, when the temperature was a little less than 200 MeV, the entire universe was perhaps filled up with the QGP or a

QGP-like state [8–11]. Current high-energy heavy-ion experiments are trying to recreate the same sequence of events, although in the reverse order, by colliding two heavy-nuclei under the controlled conditions of a laboratory. The expectation is to create a temperature and material density similar to that prevailed around 10^{-5} sec after the birth of our universe. In laboratory such a state however occupies a tiny volume, typically $\sim 10^2 - 10^3$ fm^3, and is going to survive momentarily for a time ~ 50 fm/c. We may call this event *a little bang*, a very small replica of its much bigger cosmological counterpart.

With progressing advancement in the technology sector, powerful accelerators have become available. It is possible to collide two heavy-nuclei with each other at really very high-energies, at velocities very close to that of the light, and produce thereby a large number of new particles in the final state. Depending on the collision energy and the size of the interacting nuclei, the average number of the newly produced particles, most of which are π-mesons, can be anything between 10^2 and 10^4 per collision, much larger than the corresponding numbers produced in proton-proton collisions at similar energies. The process by which these new particles are produced, is known as multiparticle production. A large nucleus consists of many nucleons. In a high-energy collision between two such nuclei, individual nucleons belonging to one of the impinging nuclei are bound to suffer many rescattering with those belonging to the other, as well as with the hadrons/partons produced thereof. While the rescattering allows sufficient time for randomization of the micro-states accessible to the produced particles, a large average number of particles in the final state results in a small relative fluctuation in thermodynamic parameters. These two factors facilitate achieving a local thermal and chemical equilibrium, so that the intermediate stage of the colliding nuclei, in spite of the small volume that it occupies and the brief time interval for which it survives, can be treated as a well equilibrated thermodynamic state. If during the collision the nucleons are sufficiently compressed and heated up, then the boundaries of individual nucleons may melt down to coalesce into a new, exotic and extended state of deconfined quarks and gluons. To detect QGP formation from the debris of hundreds and thousands of particles in the final state, is not an easy task.

Strongly interacting matter has a rich phase structure, which includes a nuclear liquid phase, a hadronic gas phase, and the QGP. All these states are described by the rules of QCD, the theory of quarks, gluons and strong interaction. It is very pertinent to ask how do the collective and macroscopic properties of nuclear/hadronic/QGP matter emerge from the interactions of elementary quarks and gluons that constitute only the individual hadrons. With the help of QCD, high-energy heavy-ion interaction tries to address this issue under high-temperature and/or high-density conditions that are accessible to the experiments. QCD is a non-abelian gauge-field theory that is based on Yang and Mills $SU_c(3)$ color symmetry. Gluons, the color carrying gauge-bosons associated with the field, are self-interacting.

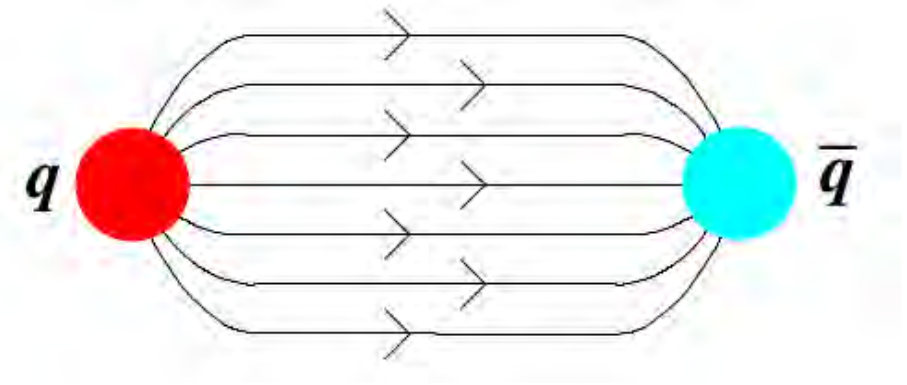

Figure 1.2: Chromoelectric flux between a $q\bar{q}$ pair [13].

Color-confinement and asymptotic freedom are two special properties of quarks and gluons. The interaction between a quark and an antiquark can be phenomenologically modelled by the so called Cornell potential [12],

$$V_s(r) = -\frac{4\alpha_s}{3r} + \kappa\, r \tag{1.1}$$

where $\alpha_s\,(= g_s^2/4\pi \approx 1)$ is the dimensionless strong coupling constant, r is the inter-quark spacing, and κ describes the long-range interaction. At short distances, or equivalently at large momentum transfers, the $1/r$ term dominates. Under such circumstances the quark - quark (qq) or the quark - anti-quark ($q\bar{q}$) interaction can be understood in terms of single gluon exchange or excitation of a single color string. With increasing distance more and more potential energy is stored within the intervening space, that can be viewed as a flux tube of color strings (see Figure 1.2). As the gluons are self-coupling and strong interaction is attractive in nature, the strings squeeze each other. As a result the color-force field effectively becomes uniform in the intervening space between the qq or the $q\bar{q}$ system. Therefore, in principle, infinite amount of energy should be required to separate one quark or anti-quark from the other. This in essence is the idea behind the permanent confinement of color degrees of freedom. On the other hand, if quantum effects are taken into account, the running (effective) coupling constant of QCD depends on the scale at which it is measured [14–16]. The dimensionful effective coupling constant in its leading order is given by,

$$g_s^2(q^2) \simeq \frac{16\pi^2}{\beta_0 \ln \frac{q^2}{\Lambda_{qcd}^2}} \quad ; \qquad \beta_0 = \frac{11}{3} N_c - \frac{2}{3} N_f \tag{1.2}$$

where q is the 4-momentum transfer, Λ_{qcd} ($\sim$ 200 MeV) is the QCD renormalization parameter, N_c and N_f are respectively the numbers of color and flavor degrees of freedom. As $\beta_0 > 0$, with increasing q^2 the QCD coupling constant decreases logarithmically. At large momentum transfer, i.e. at small distances the qq or $q\bar{q}$ interaction potential becomes

weak, which basically is the essence of asymptotic freedom [17, 18]. In the limit $q^2 \gg \Lambda^2_{qcd}$ perturbative QCD can be employed, when $q^2 \sim \Lambda^2_{qcd}$ non-perturbative methods are required.

1.2 Nucleus-nucleus collision at high-energy

In high-energy collisions involving protons and/or electrons, the incident beam energy goes into a very small volume (a few – several fm^3) equivalent to a point. On the other hand, in heavy-ion interactions a large amount of energy is deposited into an extended region of space ($10^2 - 10^3$ fm^3) within a time of a few fm/c, creating thereby a system known as the intermediate fireball. Depending on the initial conditions, the fireball energy density can rise to such a high value that new forms of matter may be created. As mentioned above, the search for such new phase(s) is the central objective of studying heavy-ion interactions. The history of high-energy nucleus-nucleus (AB) collisions dates back to the 1970s. There can be two types of AB experiments. One is called the fixed target experiments, where one of the colliding nuclei remains fixed in the laboratory. In the other, called the collider experiments, both the colliding nuclei are made to move towards each other from opposite directions. The advantage of collider facilities is that at the same incident beam energy (E), the energy available in the center of momentum system is much higher in magnitude ($\sim E$) than that available in a fixed target facility ($\sim \sqrt{E}$). The disadvantage is that, in colliders the collision rate is lower by a factor of $10^2 - 10^3$ than that in the fixed target experiments.

The first major attempt to study nuclear matter under extreme conditions was made at the Lawrence Berkeley Laboratory (LBL) by using the Bevalac facility. In those days the experimental scenario on AB interactions was dominated by the fixed target programs like, (i) the Bevatron at LBL, (ii) the Synchrophasotron (Synchro) at Joint Institute of Nuclear Research (JINR), (iii) the Alternating Gradient Synchrotron (AGS) at Brookhaven National Laboratory (BNL) and (iv) the Super Proton Synchrotron (SPS) at CERN. Though the JINR Synchrophasotron was commissioned before the Berkeley Bevelac, it was used to accelerate only the lighter ions. Both in the SPS and AGS, the facilities for accelerating nuclei came first at the late 1980's (lighter nuclei), and then again in the early 1990's (heavy nuclei). In both facilities many fixed target experiments were carried out, with a typical incident ion energy of a few hundred GeV per nucleon at the SPS, and $\sim$ 10 GeV per nucleon at the AGS. Several indicators that can identify a probable QGP $\rightarrow$ hadron phase transition, have been rigorously examined by analyzing the data available from these experiments. The experimental results have been compared with the models based on numerical simulations, the theories were modified and the results were repeatedly examined. Despite some experimental results suggesting early signal(s) of QGP formation [19, 20], no solid evidence of a colour deconfined state was available in the fixed target

experiments, thus eluding the expectations of a large number of researchers working in this field. In the beginning of the 21st century the experimental study of high-energy heavy-ion collision entered into a new era, when the Relativistic Heavy-Ion Collider (RHIC) started functioning at the BNL. This was followed by the establishment of the Large Hadron Collider (LHC) at CERN, making provision for a collision energy higher than that available in the RHIC by an order of magnitude. For the first time, in any terrestrial laboratory the experiments at RHIC and LHC started to indicate formation of a color deconfined extended QCD state like the QGP at high temperature and low baryonic potential. The data analysis, refinement of accumulated results, and physics analysis are still going on. Some of these results are going to be very briefly discussed later in the experimental review section of this chapter. To complement the RHIC and LHC experiments and to study the QCD state at high baryochemical potential, the Compressed Baryonic Matter (CBM) experiment is being designed and comissioned at the Facility for Anti-proton and Ion Research (FAIR) at GSI, Darmstadt [21]. Over the past forty years or so, there has been a tremendous advancement in the technology sector. As a result, there has been a $10^3 - 10^4$ times increase in the collision energy. The major heavy-ion programmes undertaken till date are listed in Table 1.1. The list will help us understand the chronology of this development in terms of the past, present and future accelerator facilities.

A nucleus consists of A nucleons. In the ground state it occupies a volume $V = 4\pi r_0^3 A/3$. It has a matter density

$$\rho = \frac{3}{4\pi r_0^3} \tag{1.3}$$

and it possesses an energy density

$$\epsilon = \frac{A \times m_N}{V} \tag{1.4}$$

Here $r_0 = 1.15$ fm is the nuclear radius parameter, and $m_N = 0.94$ GeV/c^2 is the nucleon rest mass. Typical values are $\rho \approx 0.16$ nucleons/fm^3 and $\epsilon \approx 0.15$ GeV/fm^3. Whatever may be the constituent particles, if the intermediate fireball created in an AB collision has to qualify as a state, it should have well defined values of temperature, volume, pressure etc.. This is possible only when the motion of the constituent particles, after experiencing multiple rescattering, is sufficiently random. An order of magnitude calculation in this regard may be useful to realize the context. A hadron typically has a radius of 1 fm and it fills up a volume of $5 - 6$ fm^3. So the hadronic matter density is about $n \sim 0.2$ per fm^3. Typical cross-section of a high-energy hadronic interaction is $\sigma \sim 50$ mb or ~ 5 fm^2. Collisions between two heavy-nuclei increase the density by a few orders of magnitude. As a result the hadronic density increases to $n \sim 10$. The mean free path of the constituent particles will therefore be $\lambda \sim (n\sigma)^{-1} \approx 0.02$ fm. Therefore, one can expect multiple ($\sim 10^3$) hadronic rescattering taking place within a collision volume of dimension $10 - 15$ fm, which with all

Table 1.1: Accelerator facilities in relativistic heavy-ion physics..

Accelerator	Start Year	Projectiles	Max. Energy	Experiment	Status
Bevalac Berkeley	1984	^{238}U,^{84}Kr, ^{40}Ca,^{12}C	<2A Gev	Fixed target	Closed
Synchro. JINR, Dubna	1975	^{12}C,^{24}Mg, ^{20}Ne,^{28}Si	4.5A Gev	Fixed target	Closed
BNL-AGS Brookhaven	1986	^{28}Si	14.6A Gev	Fixed target	Closed
BNL-AGS Brookhaven	1992	^{197}Au	11A Gev	Fixed target	Closed
CERN-SPS Geneva	1986	^{16}O,^{32}S	200A Gev	Fixed target	Closed
CERN-SPS Geneva	1994	^{208}Pb	200A Gev	Fixed target	Closed
GSI-SIS Darmstadt	2002	^{84}Kr,^{197}Au	2A Gev	Fixed target	Operational
BNL-RHIC Brookhaven	2002	^{39}Cu,^{197}Au	$\sqrt{s_{NN}}$=200 GeV	Collider	Operational
CERN-LHC Geneva	2008	^{16}O,Ar,Pb	$\sqrt{s_{NN}}$ =5.5 Tev	Collider	Operational
GSI-SIS300 Darmstadt	2017	^{59}Ni,^{197}Au	45A Gev	Fixed Target	Operational
NICA JINR,Dubna	2017	^{197}Au,^{238}U	$\sqrt{s_{NN}} \sim 5$ GeV	Collider	Operational

probability will lead to equilibration. The thermodynamic conditions of the intermediate fireball that can be and have been reached in high-energy heavy-ion experiments using the above mentioned accelerator facilities, are listed below [22].

1. Temperature: $T = (100 - 1000)$ MeV (1 MeV $\equiv$ 10 billion degrees) [up to a million times the temperature of the core of the sun].

2. Pressure: $P = (100 - 300)$ MeV/fm^3 (1 MeV/fm$^3 \equiv$ 1028 atm.) [pressure at the center of the earth = 3.6 million atm.].

3. Density: $\rho = (5 - 10)\rho_0$ [ρ_0 is the density of a gold nucleus $\sim$ 3000 g/cm^3; density of a gold atom = 19 g/cm^3].

4. Volume: nearly 1500 fm^3, nucleus radius $R = 1.15 \times A^{1/3}$ fm [for an Au-nucleus $A \approx 200$, $R \simeq 7$ fm and $V = 4\pi R^3/3 \simeq 1500$ fm^3].

5. Duration: $(10 - 50)$ fm/c $\sim 10^{-22}$ sec.

6. Baryochemical potential: $\mu = (400 - 600)$ GeV.

7. Magnetic field: $B \sim 10^{15} - 10^{16}$ Tesla [in neutron stars $B \sim 10^{11}$ Tesla].

1.2.1 Kinematics of high-energy interaction

Let us now discuss the kinematics of two-body interaction and some variables that are commonly used to characterize the particle production process in high-energy interactions. A detailed account of the topic can be found in [23, 24]. If otherwise not mentioned we shall stick to the natural unit system ($\hbar = c = k_B = 1$). Let us consider a two body collision where the projectile has a momentum $\bar{p_1}$, energy E_1 and rest mass m_1. On the other hand the target, fixed in the laboratory system (LS), has a rest mass m_2 only. The 4-momenta of these particles are respectively,

$$p_1 = (E_1, \bar{p_1}), \text{ and } p_2 = (m_2, \bar{0}) \tag{1.5}$$

In the center of momentum (CM) frame the momentum of two interacting particles are equal but oppositely directed. Let their 4-momentum in the CM frame be denoted by,

$$p_1^* \;=\; (E_1^*, \bar{p_1^*}), \text{ and } p_2^* \;=\; (E_2^*, \bar{p_2^*} = -\bar{p_1^*}) \tag{1.6}$$

The total energy ($\sqrt{s}$) available in the CM frame is equivalent to the invariant mass of the CM. The total 4-momentum in the CM frame is

$$(p_1^* + p_2^*)^2 \;=\; (E_1^* + E_2^*)^2 - \left(\bar{p_1^*} + \bar{p_2^*}\right)^2 \;=\; (E_1^* + E_2^*)^2 \;=\; E_{cm}^2 \equiv s \tag{1.7}$$

The total 4-momentum in the LS is

$$(p_1 + p_2)^2 \;=\; m_1^2 + m_2^2 + 2E_1 m_2 \tag{1.8}$$

The 4-momentum square of any system should be a Lorentz invariant quantity. Therefore,

$$E_{cm} \;=\; \sqrt{s} = \sqrt{m_1^2 + m_2^2 + 2\, m_2\, E_{\rm lab}} \tag{1.9}$$

where $E_{\rm lab} = E_1$ is the projectile energy in LS. It is evident that at high-energies for a nucleon-nucleon (NN) system $\sqrt{s} \sim E_{\rm lab}^{1/2}$, and the center of mass moves in the LS in the direction of $\bar{p_1}$ with a velocity $\beta_{cm}c$. Corresponding Lorentz factor $\gamma_{cm} = \left(1 - \beta_{cm}^2\right)^{-1/2}$. As $E = \gamma\, m$

$$\gamma_{cm} = \frac{E_1 + m_2}{\sqrt{s}} \qquad \Rightarrow\; \sqrt{s} \simeq E_{\rm lab}/\gamma_{cm} \tag{1.10}$$

In a collider experiment if the incident energies are very high, i.e. ($E_1,\; E_2 \gg m_1,\; m_2$) then

$$E_{cm} \simeq \sqrt{4E_1\, E_2} \tag{1.11}$$

If $E_1 = E_2 = E$ then $E_{cm} \simeq 2\,E$, and the CM energy increases linearly with E. If an AB collision is viewed as an independent superposition many elementary NN collisions then the AB collision is called incoherent. In such a case for a symmetric central collision between two identical nuclei ($A = B$), the total CM energy is related to the CM energy of an NN system ($\sqrt{s_{NN}}$) as $\sqrt{s} = A\sqrt{s_{NN}}$, and corresponding Lorentz factor given by,

$$\gamma_{cm} = \frac{E}{M} = \frac{\sqrt{s}}{2Am_N} = \frac{\sqrt{s_{NN}}}{2m_N} \tag{1.12}$$

If on the other hand, each colliding nucleus behaves like a single massive object then the collision is fully coherent. In non-central collisions between two identical nuclei, in asymmetric and coherent collisions, it is difficult to fix the effective CM frame, which depends on the impact parameter as well as on the degree of coherence of the collision. Therefore, the number of participating and spectator nucleons need to be determined first, posing extra problems particularly in soft processes. For hard processes that are more likely to be observed in the central collisions, the NN frame still works.

The rapidity variable

The rapidity variable is the relativistic measure of the velocity of a particle. It is a suitable choice to describe the dynamics of relativistic particles. It is a dimensionless quantity and can be used to locate a particle in the rapidity space. In high-energy collisions the beam line is conventionally taken along the z-axis, which may be called the longitudinal direction. The $(x-y)$ plane is called the transverse plane. It is convenient to decompose the momentum vector $\bar{p}$ in two components, one in the longitudinal direction (p_l) and another in the transverse direction ($p_t = \sqrt{p_x^2 + p_y^2}$). p_t remains invariant under a Lorentz boost given along the longitudinal direction. In relativistic heavy-ion collisions the space-time rapidity of a particle is defined as

$$y = \frac{1}{2}\ln\left(\frac{t+z}{t-z}\right) \tag{1.13}$$

where t is the time and z is the space co-ordinate of the particle along the beam direction. For particles created exactly at the center of mass of the interacting system, $y = 0$. The space-time rapidity is however experimentally not measurable. It is used mainly for theoretical calculations. Therefore, the energy-momentum rapidity is introduced as,

$$y = \frac{1}{2}\ln\left(\frac{E+p_l}{E-p_l}\right) = \frac{1}{2}\ln\left(\frac{E+p_l}{m_t}\right) \tag{1.14}$$

Here $E = \sqrt{|\bar{p}|^2 + m^2}$ and $m_t = \sqrt{m^2 + p_t^2}$ is the transverse mass of the particle. The most interesting property of the rapidity variable is that, it is additive under Lorentz boost.

As a result, the overall shape of the rapidity distribution of particles remains unchanged under a longitudinal Lorentz boost. In the nonrelativistic limit, the rapidity of a particle traveling along the longitudinal direction is equal to the velocity of the particle measured in the unit of velocity of light in vacuum. The energy E and the longitudinal momentum p_l of a particle are related to the rapidity by the relation

$$E = m_t \cosh y \qquad \text{and} \qquad p_l = m_t \sinh y \tag{1.15}$$

The energy and momentum of the CMS in the LS are respectively, $\gamma_{cm}\sqrt{s}$ and $\beta_{cm}\gamma_{cm}\sqrt{s}$. The rapidity of the CM in the LS therefore, is

$$\begin{aligned} y_{cm} &= \frac{1}{2}\ln\left(\frac{\gamma_{cm}\sqrt{s}+\beta_{cm}\gamma_{cm}\sqrt{s}}{\gamma_{cm}\sqrt{s}-\beta_{cm}\gamma_{cm}\sqrt{s}}\right) \\ &= \frac{1}{2}\ln\left(\frac{1+\beta_{cm}}{1-\beta_{cm}}\right) \end{aligned} \tag{1.16}$$

Lorentz transformation between the CMS and the LS is given by the following equations,

$$E^* = \gamma E - \gamma\beta p_l; \qquad p_l^* = -\gamma\beta E + \gamma p_l; \qquad p_t^* = p_t \tag{1.17}$$

The star marked quantities are associated with the CMS. The rapidity values of a particle in the CMS and the LS are given respectively by,

$$y^* = \frac{1}{2}\ln\left(\frac{E^*+p_l^*}{E^*-p_l^*}\right) \qquad \text{and} \qquad y = \frac{1}{2}\ln\left(\frac{E+p_l}{E^-p_l}\right) \tag{1.18}$$

Using Equation (1.17) in Equation (1.14) one gets,

$$\begin{aligned} y &= \frac{1}{2}\ln\left(\frac{E^*+p_l^*}{E^*-p_l^*}\right) + \frac{1}{2}\ln\left(\frac{1+\beta}{1-\beta}\right) \\ \Rightarrow y &= y^* + y_{cm} \end{aligned} \tag{1.19}$$

Therefore in a CMS $\rightarrow$ LS transformation the rapidity distribution remains unaltered, with the y-scale shifted by an amount equal to y_{cm}. For a fixed target experiment, the beam rapidity can be obtained by using the relation (1.15). For the beam particle p_t is zero. The rapidity of beam particle (y_1) is given by,

$$\begin{aligned} y_1 &= \cosh^{-1}\left(\frac{E}{m_1}\right) = \cosh^{-1}\left(\frac{\sqrt{s_{NN}}}{2m_N}\right) \\ \Rightarrow y_1 &= \sinh^{-1}\left(\frac{p_l}{m_1}\right) \end{aligned} \tag{1.20}$$

where m_1 is the rest mass of the beam particle.

The pseudorapidity variable

Both the energy and the longitudinal momentum of a particle are necessary to determine the rapidity of that particle. But in many experiments it is not possible to measure both. In such cases it is instead convenient to use the pseudorapidity variable (η). Suppose a particle is emitted at an angle θ with respect to the beam axis. From Equation (1.14) we get the rapidity as,

$$y = \frac{1}{2}\ln\left(\frac{(m^2+|\bar{p}|^2)^{1/2}+|\bar{p}|\cos\theta}{(m^2+|\bar{p}|^2)^{1/2}-|\bar{p}|\cos\theta}\right) \tag{1.21}$$

If the kinetic energy of the particle is very high ($|\bar{p}| \gg m$) then Equation (1.21) reduces to

$$\begin{aligned} y &= \frac{1}{2}\ln\left(\frac{|\bar{p}|+|\bar{p}|\cos\theta)}{|\bar{p}|-|\bar{p}|\cos\theta)}\right) \\ &= -\ln\,\tan\left(\frac{\theta}{2}\right) = \eta \end{aligned} \tag{1.22}$$

In terms of the linear momentum components η is expressed as

$$\eta = \frac{1}{2}\ln\left(\frac{|\bar{p}|+p_l}{|\bar{p}|-p_l}\right) \tag{1.23}$$

$$e^{\eta} = \sqrt{\left(\frac{|\bar{p}|+p_l}{|\bar{p}|-p_l}\right)} \tag{1.24}$$

and

$$e^{-\eta} = \sqrt{\left(\frac{|\bar{p}|-p_l}{|\bar{p}|+p_l}\right)} \tag{1.25}$$

From Equations (1.24) and (1.25) the following relations are obtained,

$$|\bar{p}| = p_t\cosh\eta \quad \text{and} \quad p_l = p_t\sinh\eta \tag{1.26}$$

Rapidity and pseudorapidity are interchangeable and are related to each other by,

$$y = \frac{1}{2}\ln\left(\frac{\sqrt{p_t^2\cosh^2\eta+m^2}+p_t\sinh\eta}{\sqrt{p_t^2\cosh^2\eta+m^2}-p_t\sinh\eta}\right) \tag{1.27}$$

and

$$\eta = \frac{1}{2}\ln\left(\frac{\sqrt{m_t^2\cosh^2 y-m^2}+m_t\sinh y}{\sqrt{m_t^2\cosh^2 y-m^2}-m_t\sinh y}\right) \tag{1.28}$$

η is used as an approximation of y when the angular distribution of the produced particles is measured, and only when the relation $E \cong| \bar{p} |\gg m$ holds good. In high-energy interactions the approximation $\eta \cong y$ is good for the pions and other light weight particles.

1.2.2 Geometry of nucleus-nucleus collision

In a high-energy collision the colliding nuclei look like two Lorentz contracted discs or pancakes in their CM frame, the contractions being along their directions of motion. The impact parameter of a collision lies in $0 \leqslant b \leqslant (R_A + R_B)$, where R_A and R_B are the transverse radii of the colliding nuclei. The entire set of AB events falling within this b-range is called the minimum bias sample of events. In central (peripheral) collisions b is closer to its minimum (maximum) value. The schematic of an AB collision for $b \neq 0$ is shown in Figure 1.3. In

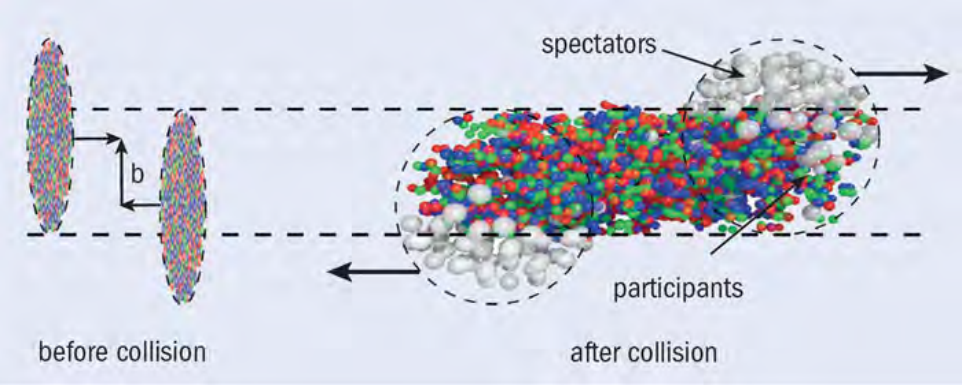

Figure 1.3: Schematic of a nucleus-nucleus collision [25].

the most peripheral collisions the interactions between the nuclei are primarily electromagnetic in nature. Either or both of the nuclei may absorb energy through giant resonances, proton-neutron clusters, higher lying nucleon resonances, and/or decay by emission of one or more nucleons. A small fraction of the total number of nucleons belonging to each nucleus are actually affected in such interactions, while most others remain unaffected. In a purely geometrical picture the cross-section of an AB reaction is given by the Bradt-Peter's formula, $\sigma_{\rm geo} = \pi r_0^2 \left(A^{1/3} + B^{1/3} - \delta\right)^2$ [26]. However, b cannot be directly measured in an experiment. Generally, any observable that varies monotonically with b can be used as its representative measure. As for example the average charged particle multiplicity N_{ch}, the total transverse energy ($E_t = \sum_i E_i \sin\theta_i$) or the energy deposited by the spectator nucleons in the Zero Degree Calorimeter ($E_{\rm ZDC}$) – the missing forward energy etc., are considered as suitable experimental measures of b. It is natural to assume that on an average, the energy released in a collision will be directly proportional to the number of nucleons participating in the collision, and the particle multiplicity will be proportional to the participating nucleon number. So the particle multiplicity is proportional to the energy liberated in the collision. For the minimum-bias event sample one can measure the N_{ch}-distribution or the E_t-distribution. High values of N_{ch} or E_t correspond to more central collisions and lower

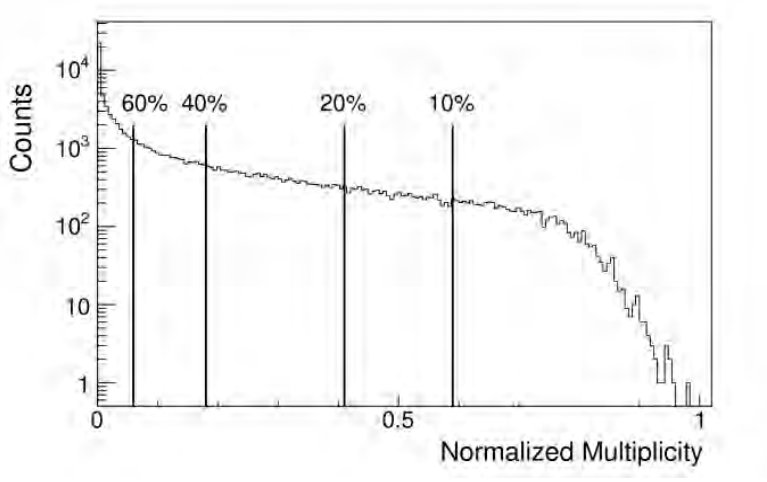

Figure 1.4: Multiplicity distribution and centrality of AB collisions.

values correspond to more peripheral collisions. The N_{ch} or the E_t distribution can therefore be utilized for the centrality determination of AB interactions. Figure 1.4 illustrates the schematic of a multiplicity distribution of charged particles for a minimum-bias event sample that can be used to assign the collision centrality. Starting from the maximum observed value of N_{ch} the area under the multiplicity distribution may be sliced into sequential intervals. The top 10% events with the highest N_{ch} values corresponds to the $(0-10)$% centrality class and so on. A similar exercise is possible for the E_t distribution too.

The Glauber model

The correlation between centrality and the number of participating nucleons has also been expounded in detail by the Glauber-type calculations using different functional forms of the nuclear density [27, 28]. The model treats an AB interaction as a superposition of multiple independent NN collisions, and at high energies the nucleons carry enough momentum to remain almost undeflected as the impinging nuclei pass through each other. It is also assumed that the nucleons move independently in the nucleus and that the size of the nucleus is large compared to the range of the NN interaction. Effectively the nucleons move on straight-line paths, and at any stage of the collision the inelastic NN cross-section ($\sigma_{\rm in}$) is assumed to be independent of the number of NN collisions that a nucleon has already suffered. In that sense it is a classical model of the interaction. As the two nuclei collide at an impact parameter $\mathbf{b}$, the probability of n inelastic NN interactions is given by,

$$P(n,\mathbf{b}) = \binom{AB}{n} \; [T(\mathbf{b})\,\sigma_{\rm in}]^n \; [1 - T(\mathbf{b})\,\sigma_{\rm in}]^{(AB-n)}$$

where $T(\mathbf{b}) = \int \rho_A(\mathbf{b}_A,\, z_A)\, d\mathbf{b}_A\, dz_A\, \rho_B(\mathbf{b}_B,\, z_B)\, d\mathbf{b}_B\, dz_B\, t(\mathbf{b} - \mathbf{b}_A - \mathbf{b}_B)$ is the normalized thickness function for the AB collision. The total probability of having an inelastic event in the collision between A and B is,

$$\frac{d^2\sigma_{\rm in}}{db^2} = \sum_{n=1}^{AB} P(n,b) = 1 - [1 - T(b)\,\sigma_{\rm in}]^{AB}$$

The total inelastic cross-section is therefore,

$$\sigma_{\rm in}^{AB} = \int 2\pi\, b\, db\, \left[1 - (1 - T(b)\,\sigma_{\rm in})^{AB}\right]$$

In the framework of the Glauber model the total number of nucleons that underwent at least one interaction ($N_{\rm part}$), or the total number of binary NN interactions ($N_{\rm coll}$) per event, can be analytically obtained as,

$$\begin{aligned} N_{\rm part}(b) &= \int d^2\mathbf{s}\, T_A(\mathbf{s})\left[1 - \exp\left(-\sigma_{\rm in}^{NN}\, T_B(\mathbf{s})\right)\right] + \int d^2\mathbf{s}\, T_B(\mathbf{s}-\mathbf{b})\left[1 - \exp\left(-\sigma_{\rm in}^{NN}\, T_A(\mathbf{s})\right)\right] \\ N_{\rm coll}(b) &= \int d^2\mathbf{s}\, \sigma_{\rm in}^{NN}\, T_A(\mathbf{s})\, T_B(\mathbf{b}-\mathbf{s}) \equiv \sigma_{\rm in}^{NN}\, T_{AB}(\mathbf{b}) \end{aligned} \tag{1.29}$$

where $T_A(\mathbf{s}) = \int dz\, \rho_A(z,\, \mathbf{s})$ is the thickness function for the nucleus A, $T_B(\mathbf{s})$ is the same for the nucleus B, and $T_{AB}(\mathbf{b})$ is the nuclear overlap function. It is assumed that an NN interaction takes place if the inter-nucleon distance d in the plane orthogonal to the beam-axis satisfies the condition $\pi\, d^2 \leqslant \sigma_{\rm in}$. An arbitrary number of such AB collisions can be generated by the Monte Carlo Glauber model [29] and the resulting distributions of $d\sigma/N_{\rm part}$, $d\sigma/N_{\rm coll}$ and $d\sigma/db$ are obtained. The systematic uncertainties in the mean values of $N_{\rm part}$ and $N_{\rm coll}$ for each centrality class are estimated by varying the parameters of nuclear density function, by varying the value of $\sigma_{\rm in}$, and from the uncertainty in the determination of the total AB interaction cross-section. These sources of uncertainties are treated as fully correlated in the final systematic uncertainty in the above measured variables. If certain cross-sections scale with the number of participants, they are associated with soft or small momentum transfer processes – the low-p_t hadron production, which accounts for almost 95% of the bulk hadron multiplicity, are phenomenologically described by non-perturbative models. On the other hand, in the hard QCD processes, like the jet formation, heavy flavor production etc., the cross-section scales with the number of primordial NN collisions $N_{\rm coll}$. In a particular centrality class $N_{\rm part}$ grows like A, whereas $N_{\rm coll}$ grows like $A^{4/3}$, hence $N_{\rm coll}$ is always equal to or higher than $N_{\rm part}$. Sometimes, the charged particle multiplicity is given in terms of the contributions of both soft and hard processes by a two-component model [30, 31] like,

$$N_{ch} = f \times N_{\rm part} + (1 - f) \times N_{\rm coll} \tag{1.30}$$

where f, typically valued at $85 - 90\%$, is the fractional contribution from soft processes.

1.2.3 Stopping in nucleus-nucleus collision

In an AB collision each incoming nucleus may be considered as a coherent cloud of nucleons. As the nuclei collide the nucleons undergo successive collisions, and transverse degrees of freedom are excited. A significant fraction of the incoming kinetic energy is deposited in the central region. This leads to the formation of a high-energy, high-density fireball, a state not anywhere close to the equilibrium. A finite amount of proper time (a few fm/c) is needed to liberate the partons in this state. Subsequent collisions lead to a locally thermalized state, which again takes a few fm/c of proper time. If the incident energy involved is extremely high, i.e. $\gtrsim$ the highest RHIC energy, the participating nucleons are far apart in the phase space. Under such a condition the colliding nuclei are to a large extent transparent to each other. Significant amount of energy will still be deposited in the central rapidity region, which is used to form $q\overline{q}$ pairs. Baryons become as abundant as the antibaryons and the net baryon content of the state becomes small. Most of the final state particles are produced in the form of mesons. This may eventually lead to a QGP at high-temperature and low chemical potential. A similar state perhaps has already been created in the RHIC and LHC experiments. The system subsequently evolves like a relativistic imperfect fluid. Models based on perturbative QCD and hydrodynamics are used to theoretically study such states. Nuclear stopping measures the efficiency of slowing down the incoming nucleons and the ability to convert the incoming kinetic energy to transverse degrees of freedom. If the stopping is high, the total baryon number carried by the interacting nucleons is significantly redistributed, leading to a high baryo-chemical potential of the equilibrated fireball. The underlying physics issues are addressed by non-perturbative QCD and/or hadronic transport models. The stopping is large when a complete overlap between the projectile and target nuclei is achieved. It is measured by the average rapidity loss as [24],

$$\langle \delta y \rangle = y_{_P} - \langle y_{_B} \rangle = y_{_P} - \frac{2}{N_{part}} \int_0^{y_P} y \, \frac{dN_{_{B-\overline{B}}}}{dy} \, dy \tag{1.31}$$

where $\langle y_{_B} \rangle$ is the net average baryon rapidity after the collision. The average scaled rapidity shift does not significantly change up to the SPS energy. We find $\langle \delta y / y_{_P} \rangle \approx 0.27$ at $E_{lab} = 200A$GeV [32]. For comparable system size the normalized rapidity density does not change with beam energy. Corresponding energy loss (ΔE) is

$$\Delta E = \int_{-y_P}^{y_P} \langle m_{_t}(y) \rangle \, \frac{dN_{_{B-\overline{B}}}}{dy} \, \cosh y \, dy \tag{1.32}$$

which comes out to be $\Delta E = 25.7 \pm 2.1$ TeV at the top RHIC energy [33]. It should also be noted that an incomplete stopping and a longitudinally expanding source lead to similar rapidity distributions.

The energy available for particle production in an AB collision depends globally on $\sqrt{s_{NN}}$ and collision centrality, and locally on p_t and y. The p_t-spectra of produced particles can in general be divided into a low-p_t and a high-p_t part. The low-p_t part is due to the random kinetic and collective motion of the particles present in the fireball, which has a thermal origin and can be described by an exponentially decaying function. The high-p_t part on the other hand, is dominated by hard processes and can be described by a power-law. The inverse slope of the p_t-spectrum is the effective temperature (T_e) of the source from which the particles are originating. T_e can be measured from our knowledge of the p_t-distribution. If the distribution can be approximated as exponentially decaying, then for $\langle p_t \rangle \gg m$ one gets $\langle m_t \rangle \approx \langle p_t \rangle \approx 2T_e$. Integrating the invariant yield over the entire p_t region one gets the rapidity distribution dN/dy of produced particles. Significant amount of information on AB collisions can be extracted by studying the rapidity distribution. Particle identification is necessary for rapidity measurement, which may not be possible in all experiments. Under such circumstances the pseudorapidity distributions are used. At very high-energies dN/dy should exhibit a plateau, which due to the transformation given in Equation (1.28) gets depleted by a small extent around $\eta^* = 0$. In the CMS the depletion factor reads as $(1 - m^2/ < m_t^2 >)^{1/2}$, whereas in the LS the peak of the distribution is located at around half of the beam rapidity ($y_P/2$), and the depletion factor is $[1 - m^2/ \{< m_t^2 > \cosh^2(y_P/2)\}]^{1/2}$. Due to the additive property of the rapidity variable under Lorentz boost, the rapidity distribution remains unchanged as one moves from one reference frame to the other. In any relativistic AB collision usually there is a central particle producing region which results from the nucleons directly participating in the collision, and two baryon rich fragmentation regions (target and projectile) dominated by the spectator nucleons. If the colliding nuclei are transparent with respect to each other, they leave a trail of energy in the form of stretched out strings. The strings subsequently fragment and the central region is populated mostly by different types of mesons. Apart from a down-shift in their rapidity values necessary to conserve energy, the baryons (nucleons) continue to move out of the central rapidity region. On the other hand when the colliding nuclei substantially stop each other, the central rapidity region is filled up with both energy and baryons. Under complete stopping the projectile and target nucleons loose all memories of their initial states. Correspondingly, the difference (if there is any) between the energy and baryon number distributions in longitudinal and transverse directions with respect to the collision axis is very little. These two extreme situations are schematically represented in Figure 1.5. The difference between the rapidity values of the projectile and the target, $\Delta y = y_P - y_T$ is important for characterization of the central region. For targets fixed in

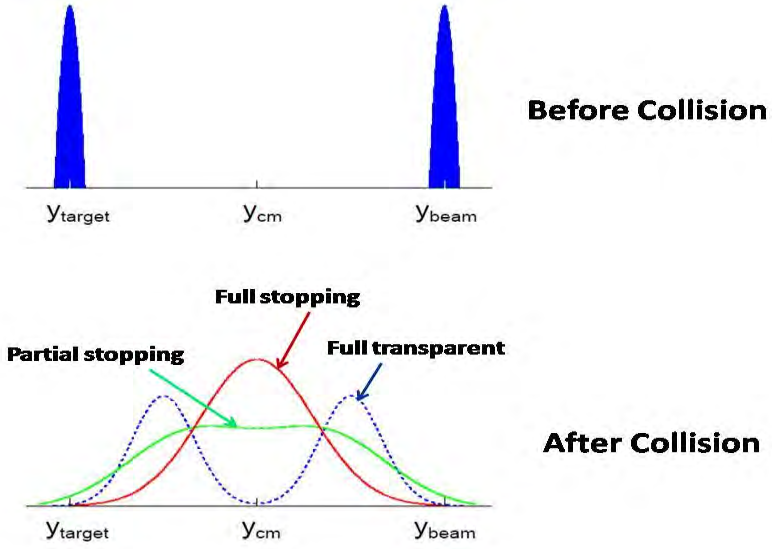

Figure 1.5: Stopping in nucleus-nucleus collisions.

the LS, $y_{_T} = 0$ and $\Delta y = y_{_P}$. Accordingly $\cosh \Delta y = E_{_P}/m_{_P}$. In a symmetric collider experiment the CMS is at rest in the LS, and for a head on collision $\Delta y/2$ is the rapidity of the projectile/target. With increasing $\sqrt{s_{NN}}$ the rapidity gap increases as, $\Delta y \propto \ln \sqrt{s_{NN}}$ [34]. This enables us to study the central region without actually having to account for particles spilling over from the fragmentation regions. Up to the SPS energy the rapidity distribution does not show any plateau and can in stead be described by a single Gaussian curve having a width $\sigma(y) \simeq 2 - 3$ rapidity units. Any system having a preferentially longitudinal expansion of the particle emitting source, will therefore have a reasonably large rapidity gap ($\Delta y > 3$), which occurs beyond the SPS energy. Experimental data suggest that nuclear/partonic stopping is present in the primordial, first generation collisions at the microscopic level. Rapidity distributions of particle multiplicity and/or transverse energy exhibit qualitatively similar shape, which on one hand evolve similarly with $\sqrt{s}$ in pp, $p\bar{p}$ and e^+e^- reactions, and in central AB collisions on the other. For the bulk hadron rapidity distributions one can formulate a nuclear modification factor [24] as,

$$R_{AA}(p_t) = \frac{1}{\langle N_{coll} \rangle} \times \frac{\frac{d^2N_{AA}}{dp_t\, dy}}{\frac{d^2N_{pp}}{dp_t\, dy}} \tag{1.33}$$

The numerator of the ratio is the single particle p_t-distribution in a symmetric AA collision, while the denominator part is the single particle distribution of the same species of particles produced in pp collisions at the same incident energy per nucleon. In the above we assume that the AA collision is an incoherent superposition of many binary NN collisions. If the contribution to the total particle yield from each NN pair is considered to be same as that coming from a pp collision at the same $\sqrt{s}$, then $R_{_{AA}} = 1$. However, in RHIC and LHC experiments $R_{_{AA}}$ is found to be larger than unity, indicating thereby a higher stopping in

nuclear collisions.

1.2.4 Evolution of nucleus-nucleus collision

The fireball system created in a high-energy heavy-ion collision passes through several different stages. Different probes that are sensitive to different stages of its space-time evolution, are used to determine the properties of the fireball. A schematic of different stages of an AB collision process is shown in Figure 1.6, and a brief qualitative description of each stage is sequentially summarized below.

- **Pre-equilibrium stage -** The initial AB collision takes place within a time span of $2R/\gamma_{cm}$, where R is the nuclear radius and γ_{cm} is the Lorentz factor in the CMS. For symmetric and central collisions between two heavy-nuclei, this amounts to a passing time of the order of a few fm/c. As for example in a $Au + Au$ or a $Pb + Pb$ collision at $E_{lab} = 200$ GeV the γ_{cm} factor ~ 10 and $2R/\gamma_{cm} \simeq 1.4$ fm/c. The initial stage of the collision is labeled as the pre-equilibrium stage. Processes like parton-parton hard scattering predominantly take place in the overlap region of the colliding nuclei, depositing thereby a large amount of energy in the central ($z \sim 0$) region. This stage can be investigated by using high-p_t probes such as jets, heavy-quarks and direct photons. During this stage intense matter compression and heating take place.

- **Equilibration of the fireball -** After the short pre-equilibration stage a fireball is created. Depending on the initial conditions due to multiple rescattering among the participating nucleons, thermal equilibrium may be established. In relativistic hydrodynamical models the equilibration process is very fast. It takes place within ~ 1 fm/c, while lacking an exact mechanism for this to happen. If the matter and/or energy density is sufficiently high, a QGP-like state may also be formed, which will be dominated by parton-parton and/or string-string scattering. The transition from the QGP to a hadron gas may occur at and around the Hagedorn limit of temperature $T_H \approx 170$ MeV [35–37]. After a local thermal equilibrium is achieved, due to an extremely large pressure gradient against the surrounding vacuum, the fireball system starts expanding. Relativistic hydrodynamics describes the evolution of the system. The specific viscosity of the system, though may not exactly vanish, is very close to its ideal limit, making the expansion to behave almost like a perfect fluid.

- **Chemical freeze-out -** As the system expands, it cools down until the temperature drops below a critical value, T_c say. It induces a phase transition causing the quarks and gluons to recombine and form color neutral hadrons. The expanding fireball first reaches a chemical freeze-out stage when the inelastic interactions between the partons

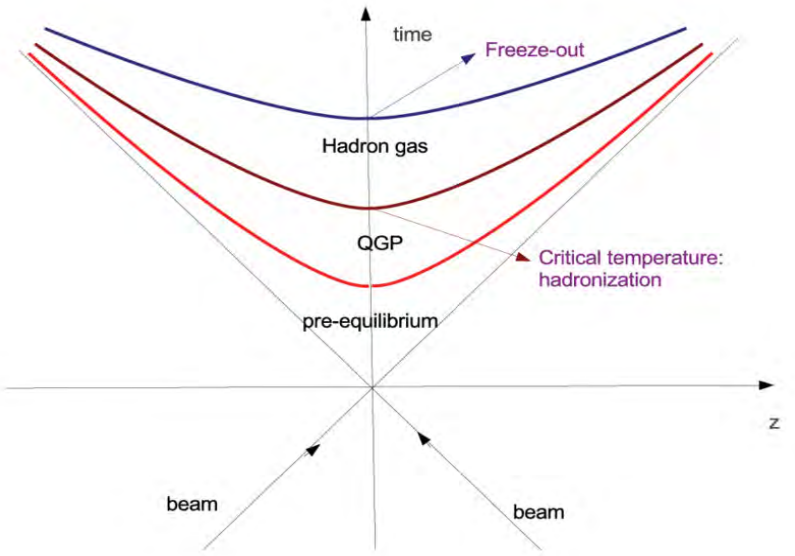

Figure 1.6: Illustration of space-time evolution of an AB collision.

cease to take place, and the relative abundance of every single particle species does not change anymore. It is considered as a mixed phase that exists between the QGP and hadronic gas. The entropy density is transferred to lower degrees of freedom and therefore, the system is prevented from a fast expansion and cooling due to the softest point defined by a minimum value of the energy density/pressure (ε/p) ratio in the equation of state. The exact mechanism of hadronization is yet unknown. Due to inelastic interactions the system can still maintain local thermal equilibrium.

- **Kinetic freeze-out -** In the hadronic phase the system maintains a collective expansion via hadron-hadron elastic interactions, thereby further decreasing the temperature of the fireball. The thermal or kinetic freeze out is triggered by this expansion, when the time scale associated with the collision mean free path of the particles becomes larger than the time scale associated with the collective expansion. As a result the elastic collisions between the particles slow down, a strongly coupled system evolves into a weakly coupled one, and the final state particles freely stream out from the fireball medium.

1.2.5 Thermodynamics of the fireball

It was none other than E. Fermi who first applied statistical physics and thermodynamics to multiple meson production in high-energy collisions [38]. Fermi assumed that when two nucleons collide, they release their energies within a very small volume $V = 2m_N V_0/\sqrt{s_{NN}}$, where $V_0 = 4\pi R_\pi^3/3$ and $R_\pi = 1/m_\pi$ is the characteristic length (Lorentz contracted)

associated with the pion field. At the instant of collision, a large number of particles are formed. The mean free path of these particles is small compared to the dimension of the interaction volume, and a statistical equilibrium is set up. Subsequently the system decays into one of the many accessible multiparticle states. The decay probability is calculated in the framework of standard statistical physics. The main reason for the introduction of statistical concepts was the breakdown of perturbation theory in describing strongly interacting systems. A large value of the coupling constant prohibits any application of perturbative methods. On the other hand, the large coupling is responsible for multiparticle production, which is a very characteristic feature of strong interaction. The transition probability from an initial to a given final state is proportional to the modulus square of the transition matrix element and to the density of states. The matrix element is treated as a constant. The main effect comes from the available phase space, which grows with increasing collision energy. The probability of having an n-particle final state is proportional to

$$S(n) \;=\; \left[\frac{V}{(2\pi)^3}\right]^{(n-1)} \frac{dN}{dE}$$

Here dN/dE is the density of states. The power $(n-1)$ comes because only $(n-1)$ particles have independent momentum. Fermi argued that at very high energies even a detailed statistical description may not be necessary [38]. Assuming that the matter is thermalized, one can calculate the temperature of the produced hadronic system from thermodynamic considerations valid for massless particles. Fermi considered production of pions, nucleons and antinucleons, and obtained the total energy density in the center-of-mass frame as,

$$\varepsilon \;=\; \varepsilon_{\pi} \,+\, \varepsilon_{N+\bar{N}} \;=\; \frac{\pi^2 T^4}{3}$$

Using the expression for the Lorentz contracted volume we may rewrite the above relation,

$$T^4 \;=\; \frac{3\,\varepsilon^2}{2\pi^2 V_0\, m_N} \;=\; \frac{9\varepsilon^2 m_{\pi}^3}{8\pi^3 m_N}$$

This equation may be used to calculate the abundance of produced particles from the thermodynamic relations giving the particle densities in terms of temperature.

As mentioned above a transition from the color neutral hadrons to the color conducting plasma consisting of nearly free quarks and gluons, can be accomplished through high-energy heavy-ion interactions. Using the accelerator facilities like RHIC and LHC it is possible to create such transient states of high energy and/or matter density that have definite equilibrium properties. The fireball however is not a static system and it evolves with space-time. It has been experimentally established that the fireball behaves more like an imperfect fluid possessing a small but finite viscosity, rather than like an ideal gas. To

begin with a static idealization of the fireball system would still be quite instructive, which has been done below in the framework of the MIT bag model [39]. Complexities and finer details that are needed for a more realistic system can gradually be added on at later stages.

In the MIT Bag model a hadron is considered to be a closed spherical bag of radius R composed of non-interacting quarks and/or anti-quarks. Due to the presence of the quarks (anti-quarks) the normal QCD vacuum is destroyed within the bag and we have a perturbative QCD vacuum inside. Energy and momentum conservation at the bag surface is ensured by introducing an external pressure at the bag surface to balance the internal pressure of the confined quarks. Each quark and/or antiquark is a spin$-\frac{1}{2}$ Fermion, massless inside the bag but infinitely massive outside. Therefore, each quark (antiquark) can be described by Dirac's equation for a massless free particle. Using the MIT bag model we can arrive at the thermodynamic conditions necessary to create the QGP [23]. To begin with we treat the quark (anti-quark) system as an ideal relativistic gas of massless ($\epsilon = pc$) Fermions at an equilibrium temperature T. The number density n_q of quarks in such a system can be derived by using the Fermi-Dirac distribution,

$$n_q \;=\; g_q \left(\frac{1}{2\pi}\right)^3 \int_0^\infty \frac{1}{e^{(p-\mu_q)/T}+1}\, 4\pi p^2 dp$$

The corresponding energy density ε_q is

$$\varepsilon_q \;=\; g_q \left(\frac{1}{2\pi}\right)^3 \int_0^\infty \frac{p}{e^{(p-\mu_q)/T}+1}\, 4\pi p^2 dp$$

Here μ_q is the quark chemical potential, and the quark-degeneracy factor

$$g_q \;=\; g_{spin} \;\times\; g_{color} \;\times\; g_{flavor}$$

is same as that ($g_{\bar{q}}$) of the anti-quark. If only two flavors (up and down) constitute the gas then $g_q \;=\; g_{\bar{q}} \;=\; 12$, and if three flavors (up, down and strange) are involved then $g_q = g_{\bar{q}} = 18$. For $\mu_q \neq 0$ neither of the above integrations can be individually worked out because the quark number density is not fixed, though the difference between the quark and anti-quark number density is. Moreover, as a quark can annihilate an anti-quark to produce a quantum of radiation, for a baryon-free gas one can write $\mu_q + \mu_{\bar{q}} = 0$. Presence of an anti-quark of energy ϵ in the gas system can be viewed as the absence of a quark of energy $-\epsilon$. Therefore, the corresponding expressions for an ideal anti-quark-gas will be

$$\begin{aligned} n_{\bar{q}} \;&=\; g_{\bar{q}} \left(\frac{1}{2\pi}\right)^3 \int_0^\infty \frac{1}{e^{(p+\mu_q)/T}+1}\, 4\pi p^2 dp \\ \varepsilon_{\bar{q}} \;&=\; g_{\bar{q}} \left(\frac{1}{2\pi}\right)^3 \int_0^\infty \frac{p}{e^{(p+\mu_q)/T}+1}\, 4\pi p^2 dp \end{aligned}$$

Putting the number density expressions together for an ideal massless quark and anti-quark gas we get,

$$n_q \, - \, n_{\bar{q}} \, = \, g_q \times \left(\frac{\mu_q}{6} \, T^2 \, + \, \frac{\mu_q^3}{6\pi^2} \right)$$

For a two flavor system ($g_q = 12$) we can now determine the net baryon number density as,

$$n_{_B} \, = \, \frac{n_q \, - \, n_{\bar{q}}}{3} \, = \, \frac{2\mu_q}{3} \, T^2 \, + \, \frac{2\mu_q^3}{3\pi^2} \, = \, \frac{2\mu_{_B}}{9} \, T^2 \, + \, \frac{2\mu_{_B}^3}{81}$$

since $\mu_{_B} \, = \, 3\mu_q$. Similarly we get the energy density as,

$$\varepsilon_q \, + \, \varepsilon_{\bar{q}} \, = \, g_q \times \left(\frac{7\pi^2}{30} \, T^4 \, + \, \frac{\mu_q^2}{4} \, T^2 \, + \, \frac{\mu_q^4}{8\pi^2} \right)$$

The gluons are massless and there is no conservation rule to restrict their number. The chemical potential $\mu_g = 0$. The number density and the energy density of an ideal gluon gas can be respectively obtained by using the Bose-Einstein distribution function,

$$\begin{aligned} n_g \; &= \; g_g \left(\frac{1}{2\pi} \right)^3 \int_0^\infty \frac{1}{e^{p/T} - 1} \, 4\pi p^2 dp \, = \, \frac{g_g}{\pi^2} \, \zeta(3) \, T^3 \\ \varepsilon_g \; &= \; g_g \left(\frac{1}{2\pi} \right)^3 \int_0^\infty \frac{p}{e^{p/T} - 1} \, 4\pi p^2 dp \, = \, g_g \frac{\pi^2}{30} \, T^4 \end{aligned}$$

The gluon degeneracy factor

$$g_g \, = \, 2 \, (\text{spin}) \, \times \, 8 \, (\text{color}) \, = \, 16$$

Adding the quark, antiquark and gluon energy densities together and combining the degeneracy factors we get [40],

$$\varepsilon_{qgp} \, = \, \varepsilon_q \, + \, \varepsilon_{\bar{q}} \, + \, \varepsilon_g \, = \, \left(\frac{37\pi^2}{30} \, T^4 \, + \, 3\mu_q^2 \, T^2 \, + \, \frac{3\mu_q^4}{2\pi^2} \right)$$

One expects a stable QGP when the pressure inside $P = \frac{1}{3}\varepsilon \geqslant B$, the equality holds at the boundary of stability. The condition may be used to arrive at the limiting critical values of the temperature T_c, the chemical potential μ_c and the baryon number density n_c,

$$\begin{aligned} T_c \, (\mu_q = 0) \; &= \; \left(\frac{90B}{37\pi^2} \right)^{\frac{1}{4}} \, \approx \, 147 \, \text{MeV} \\ \mu_c \, (T = 0) \; &= \; \left(2\pi^2 B \right) \, = \, 0.43 \text{ GeV} \\ n_c \, (T = 0) \; &= \; \frac{2}{3\pi^2} \, \left(2\pi^2 B \right)^{\frac{3}{4}} \, = \, 0.72 \text{ fm}^{-3} \end{aligned} \tag{1.34}$$

If the quark – quark and quark – anti-quark interactions are taken into account then the above expression of energy density is modified as [41],

$$\varepsilon = \left(\frac{37\pi^2}{30} - \frac{11\pi}{3}\alpha_s\right) T^4 + \left(1 - \frac{2}{\pi}\alpha_s\right) 3\mu_q^2 T^2 + \left(1 - \frac{2}{\pi}\alpha_s\right) \frac{3\mu_q^4}{2\pi^2}$$

Using the stability condition and setting the corresponding chemical potential μ_c and temperature T_c we get

$$B = \left(\frac{37\pi^2}{90} - \frac{11\pi}{9}\alpha_s\right) T_c^4 + \left(1 - \frac{2}{\pi}\alpha_s\right) {\mu_c}^2 T_c^2 + \left(1 - \frac{2}{\pi}\alpha_s\right) \frac{{\mu_c}^4}{2\pi^2}$$

Under the limiting conditions

$$T_c = \left[\frac{B}{\left(\frac{37\pi^2}{90} - \frac{11\pi}{9}\alpha_s\right)}\right]^{\frac{1}{4}} \quad \text{at } \mu_q = 0,$$
$$\text{and } \mu_c = \left[\frac{2\pi^2 B}{\left(1 - \frac{2}{\pi}\alpha_s\right)}\right]^{\frac{1}{4}} \quad \text{at } T = 0 \tag{1.35}$$

Depending on the values of B and α_s chosen, the critical temperature T_c would lie somewhere between $150 - 200$ MeV and the chemical potential μ_c somewhere between $450 - 600$ MeV.

1.2.6 Hydrodynamics of the fireball

Relativistic hydrodynamics provides a simple picture of the space-time evolution of the hot and dense matter produced in the central rapidity region of a relativistic AB collision. It is assumed that the expanding system stays in local thermodynamical equilibrium. Without going into the details of any microscopic aspect, hydrodynamics then allows us to describe all the stages of expansion of the fireball, starting possibly from the QGP, through hadronization and ending at the freeze out. Hydrodynamics, although classical in concept and formulation, provides an important computational tool to describe the gross features of AB collisions. It uses the fundamental conservation laws of energy and momentum to build an equation of state for the evolving system.

Landau's hydrodynamic model

Landau [42, 43] reexamined Fermi's original idea, and argued that one should not expect the number of finally emitted particles to be determined only from the equilibrium condition at the instant of collision. Rather the system remains strongly interacting even after the initial stages of the collision, and the number of particles becomes definite only when they

are far apart in phase space. Landau too assumed that a compound system is formed, and energy is deposited in a small volume V which is subjected to a Lorentz contraction in the longitudinal direction. At the instant of the collision a large number of particles are formed. In comparison with the dimension of the collision volume the mean free path of these particles is small, and a statistical equilibrium is set up. If two equal sized nuclei, each of mass number A, collide head on ($b = 0$) with each other, then the total energy of the colliding system in the center of mass frame (E_{cm}) is

$$E_{cm} = A\sqrt{s} \; = \; 2Am_N\gamma_{cm} \tag{1.36}$$

The initial energy density ε is then given by

$$\varepsilon \; = \; \frac{E_{cm}}{V} \; = \; \frac{2Am_N\gamma_{cm}}{V_{rest}/\gamma_{cm}} \; = \; 2\varepsilon_{nm}\gamma_{cm}^2 \tag{1.37}$$

where $\varepsilon_{nm} \; = \; Am_nV_{rest} \approx 0.15$ GeV/fm^3 is the energy density of nuclear matter, $V_{rest} \; = \; 4\pi R^3/3 \; = \; 4\pi r_0^3 A/3$ is the volume of each nucleus at rest, and r_0 is the nuclear radius parameter. Similarly, the initial baryon number density is

$$\rho_B = \frac{2A}{V} \; = \; \frac{2A}{V_{rest}/\gamma_{cm}} \; = \; 2\rho_{nm}\gamma_{cm} \approx 0.16\,\mathrm{GeV/fm}^3 \tag{1.38}$$

where $\rho_{nm} \; = \; A/V_{rest}$ is the baryon number density of nuclear matter. In terms of the inelasticity factor (K) the initial energy density is then given by,

$$\varepsilon \; = \; K\frac{\sqrt{s}}{V} \; = \; 2\gamma_{cm}^2 K\varepsilon_h \tag{1.39}$$

where ε_h is the energy density of a hadron. In the second stage of the collision, under the influence of a longitudinal velocity gradient the system starts expanding. The transverse gradients are also present, but initially the longitudinal gradient is predominant and the early expansion is approximated as one-dimensional. The expanding system is regarded as an ideal fluid with zero viscosity and zero thermal conductivity. During the expansion the mean free path of the particles constituting the system still remains small in comparison with the dimension of the interaction volume, and the velocities of the particles are comparable to that of the light, justifying thereby the use of relativistic hydrodynamics. Particles are formed and absorbed in the system throughout the first and second stages of the collision. As the system expands, the mean free path of the particles becomes comparable to the dimension of the colliding system, and the interaction between the particles becomes weak. The expanding system then breaks up into individual particles when its temperature $T \sim m_\pi$. For a perfect fluid only one equation of state is necessary to describe the hydrodynamic expansion. If P is the pressure and ε is the energy density of the fluid, mainly composed of pions, then

following the black body radiation law $P = \frac{1}{3}\varepsilon$. Assuming that in comparison with the temperature T the baryon chemical potential μ_B is small, we get

$$Ts = \varepsilon + P \;\; \Rightarrow \; Tds = d\varepsilon$$

where s is the entropy density. Combining the above two relations we find that

$$s \propto \varepsilon^{3/4} \quad \text{and} \quad T \propto \varepsilon^{1/4}$$

The initial energy density $\varepsilon \propto \gamma_{cm}^2$, $E_{cm} \propto \gamma_{cm}$, and $\varepsilon \propto E_{cm}^2$. As a result,

$$s \propto \varepsilon^{3/4} \propto E_{cm}^{3/2}$$

A perfect fluid does not have any viscosity and during the hydrodynamic expansion the total entropy of the system remains unchanged. According to the black-body radiation formula,

$$N_\pi \propto sV \propto E_{cm}^{3/2} V_{rest}/\gamma_{cm} \propto A E_{cm}^{1/2} \propto A E_{lab}^{1/4}$$

which implies that heavy nuclei are better suited for pion production and that pion multiplicity grows slowly with collision energy. Landau solved the hydrodynamic equations in one and three-dimensions. An exact solution was obtained in one-dimension [44] which gave the same result as Landau's in the asymptotic region.

A necessary condition for the applicability of the Landau's picture to central relativistic AB collisions is that the nucleons in the front part of each of the colliding nuclei, while traversing through the other nucleus, must loose all of their kinetic energies in the center of mass frame. This demands that the average energy loss of these nucleons per unit length should be greater than a critical value given by,

$$\left|\frac{dE}{dz}\right|_{cr} = \frac{E_{cm}/2}{(2R/\gamma_{cm})} \tag{1.40}$$

Although at low energies ($E_{cm} < 10$ GeV) Landau's theory gives satisfactory results, but at ultra-relativistic energies ($E_{cm} = 200$ GeV) the condition becomes too stringent to be attained. Hence, Landau's picture breaks down when the required stopping power becomes too large. Furthermore, in contrast to the requirements of Fermi's and/or Landau's approach, the thickness of the colliding nuclei cannot be infinitely small even in the ultra-relativistic region. Also, in this model the boundary condition is specified at the time of maximum compression, whereas the entire matter is distributed over a small but finite volume. However, particle production is not an instantaneous process and it shows the characteristics of space-time correlation – fast particles are produced later and further away from the collision

center than the slow particles, which is not taken into account in Landau's model. The main criticisms of Landau's model are that, the leading particle effect is neglected, and in order to achieve full stopping, removal of radiation energy due to deceleration is required. These difficulties can be removed if one assumes that during the collision the valence quarks move without much interaction, and the energy carried by the gluon fields is stopped within the collision volume [45–47]. The assumption is justified because, due to color degeneracy the gluon-gluon interaction cross-section is larger than the quark-quark cross-section. To be consistent with the initial condition of Landau's model the gluon field should thermalize after a certain time.

Bjorken's hydrodynamical model

Bjorken introduced a hydrodynamic model [48] that is based on the assumption that at sufficiently high-energy the rapidity distribution of the final state particles is uniform in the mid-rapidity region. The space-time evolution of the system should look essentially same in all center-of-mass frames. It is also assumed that the strongly interacting matter present within the collision volume, reaches a state of local thermal equilibrium after the collision and subsequently expands adiabatically. The evolution of the system is determined by the initial conditions, and an equation of state (EoS) that transfers the energy and baryon density to the pressure exerted by the system, and which is subjected to the constraints of local conservation of energy-momentum and currents [49, 50]. The EoS for a non-dissipative ideal fluid can be mathematically formulated as

$$\begin{aligned} \partial_\mu T^{\mu\nu}(x) = \partial_\mu[(\varepsilon(x) + P(x))u^\mu u^\nu - g^{\mu\nu}P(x)] = 0 \\ \partial_\mu j_B^\mu(x) = \partial_\mu \left[n_B(x)u^\mu(x)\right] = 0 \end{aligned} \tag{1.41}$$

where

$$T^{\mu\nu} = [\varepsilon + P]\; u^\mu\, u^\nu - g^{\mu\nu}\, P$$

is the relativistic stress energy tensor, ε is the energy density, P is the pressure, j_B^μ is the charge-current density, n_B is the baryon number density, and $u^\mu = (\gamma, \gamma\,\bar{v})$ is the four-velocity, all defined in the local rest frame (x) of the fluid. In Bjorken's theory all thermodynamic quantities characterizing the central region should depend only on the longitudinal proper time $\tau = \sqrt{t^2 - z^2}$ and longitudinal velocity $u_z = z/t = \tanh y$, so that $u^\mu = (t/\tau, 0, 0, z/\tau)$. Bjorken's equation is now transformed as,

$$\frac{\partial \varepsilon}{\partial \tau} + \frac{\varepsilon + P}{\tau} = 0 \tag{1.42}$$

Using $\varepsilon = \lambda P$, where $\lambda = dP/d\varepsilon$ measures the elastic wave velocity in the medium, and the thermodynamic relation, $\varepsilon + P = Ts + \mu_{_B} n_{_B}$, we get,

$$\varepsilon(\tau_f) = \varepsilon(\tau_i) \left(\frac{\tau_i}{\tau_f}\right)^{1+\lambda} \tag{1.43}$$

For zero baryon density,

$$s(\tau_f) = s(\tau_i) \left(\frac{\tau_i}{\tau_f}\right) \quad \text{and} \quad T(\tau_f) = T(\tau_i) \left(\frac{\tau_i}{\tau_f}\right)^{\lambda} \tag{1.44}$$

A QGP to hadron gas phase transition causes softening of the EoS. As the temperature crosses its critical value, the energy and entropy densities quickly increase while the pressure rises slowly. The derivative $dP/d\varepsilon$ has a minimum at the end of the mixed phase, known as the softest point. The diminishing driving force slows down the build-up of flow. The preliminary conditions, which are input parameters, define the initiation of the hydrodynamic evolution and the relevant macroscopic density distributions at that point of time. The hydrodynamic evolution is terminated by implementing the freeze out condition, which describes the breakdown of local equilibrium due to decreasing local thermalization rates. In non-central collisions, driven by its inner asymmetric pressure gradients, the system will expand more prominently in the direction of the reaction plane than in the direction perpendicular to the reaction plane. As the time evolves, the system becomes less and less deformed. To estimate the initial energy density of a Bjorken-type fluid element one has to go to the fluid rest frame. All particles are originating from a cylindrical volume of cross-section area A, which actually is the overlap area of the interacting nuclei, and of length $v_z t$. We concentrate on a thin slab of thickness dz centered between the two pancake-like moving nuclei. The point of impact is assumed to be the origin ($z = 0$) of our frame of reference. Therefore $dz = \tau \cosh y \, dy$, and ignoring the collisions among produced hadrons one gets the energy density as,

$$\varepsilon_{BJ} = \frac{\Delta E}{\Delta V} = \frac{E}{A}\frac{dN}{dz} = \frac{m_t}{\pi R^2 \tau}\frac{dN}{dy} = \frac{1}{\pi R^2 \tau}\frac{dE_t}{dy} \tag{1.45}$$

Taking the proper time $\tau \approx 1$ fm/c and dN/dy to be the central rapidity density of produced particles, this relation was first derived by Bjorken [48]. However, a perfect fluid must undergo an isentropic expansion, and the entropy of the expanding fireball should be a conserved quantity. In terms of the entropy density $s = S/V$ for a one-dimensional expansion. In order to compensate the Lorentz contraction, a relation like $s_i \, \tau_i = s_f \, \tau_f$ should hold between the initial and final proper time. For massless particles $\varepsilon \propto T^4$ and $s \propto T^3$. Correspondingly,

$$\varepsilon_f = \varepsilon_i \left(\frac{\tau_i}{\tau_f}\right)^{4/3} \tag{1.46}$$

which contradicts Bjorken's formula, $\varepsilon_{BJ} \sim \tau^{-1}$. The energy density formula should therefore be modified as,

$$\varepsilon = \frac{1}{\pi R^2 \tau_0} \frac{dE_t}{dy} \left(\frac{\tau_f}{\tau_i} \right)^{1/3} = 2\,\varepsilon_{BJ} \tag{1.47}$$

1.2.7 QCD phase diagram

The study of QCD phase diagram is an important and one of the primary goals of high-energy heavy-ion physics research. The QCD phase diagram shown in Figure 1.7, uses temperature (T) and baryo-chemical potential ($\mu_{_B}$) as independent variables. It shows the location of different states of nuclear, hadronic and partonic matter, indicates the type of transition from one phase to another, and marks the critical point(s) and the phase boundaries. These are some of the major issues that are still under intense investigation [51, 52]. There are two extreme conditions of QGP to hadron phase transition, (i) at high temperature and zero net baryon density, and (ii) at high baryon density and zero temperature. The $T = 0$ and $\mu_{_B} = 0$ point corresponds to the QCD vacuum. Nuclear matter exists at T close to zero and $\mu_B = 940$ MeV, the first non-vacuum state along the $\mu_{_B}$-axis and a strongly correlated super-fluid composed of non-relativistic nucleons. At a higher $\mu_{_B}$ and low T the state of matter can be described as a degenerate neutron gas, which is expected to be common in neutron stars. Since the NN interaction is somewhat like the Van-der-Waals interaction between molecules, with increasing temperature a transition similar to the liquid-gas phase transition takes place. This ends at a critical temperature $T \simeq 18$ MeV. Further heating results in a weakly interacting gas of hadronic resonances, in which the density of states grows exponentially for both mesons and baryons [35]. This suggests that hadronic matter below T_c behaves like a Hagedorn gas. One route to achieve the color deconfinement is to increase the pressure, and as such the density. Increase in pressure will push the nucleons closer until their typical size becomes larger than the average inter-nucleon distance. This will make the nucleons overlap and the boundaries of individual nucleons to melt. If the pressure is increased beyond 1 GeV/fm^3 the degenerate neutron gas no longer remains stable, because the degeneracy pressure is not sufficient to sustain a stable equilibrium. This will result in a transition to a gas of quarks, that are no longer confined within the nucleons. Further increasing the pressure is expected to result in a color superconductor. In this phase, some of the quarks will form a condensate of $q\bar{q}$ Cooper-pairs which will induce a color Meissner effect. At even higher densities the QCD interaction weakens, which opens up the possibility of a so called color-flavor locked (CFL) phase. This is a super-fluid which is an electromagnetic insulator and breaks chiral symmetry. If on the other hand, the nucleon gas is heated up to $T > 100$ MeV it becomes a hadron gas. Several hadronic species like pions and excited nucleons exist in equilibrium. Increasing the temperature further will

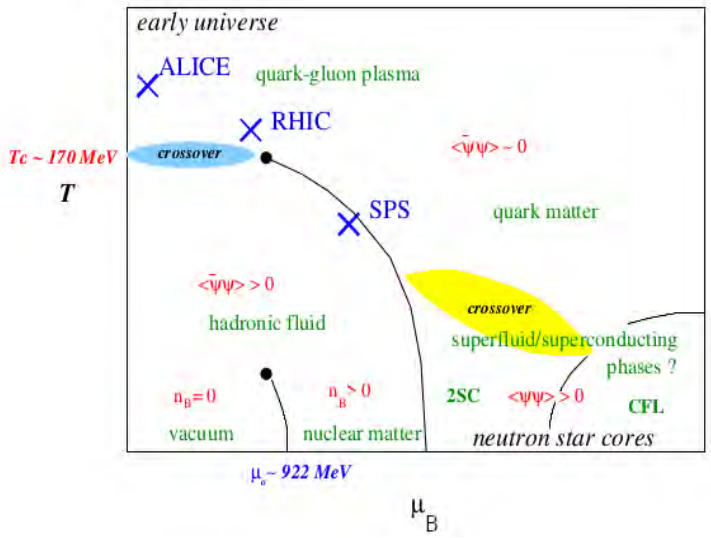

Figure 1.7: Sketch of QCD Phase Diagram [13].

cause a transition to the QGP phase. The low T and high μ_B region of the phase diagram has not been extensively studied either in experiments or in theory. We shall perhaps have to wait until the results from STAR beam energy scan program and/or CBM-FAIR become available.

The high T and low μ_B region of the QCD phase diagram has been investigated quite extensively in heavy-ion experiments held at the LHC and RHIC. The high T and low μ_B QGP should behave like a dilute gas of weakly coupled partons. However, contrary to the expectations the LHC and RHIC results suggest that the QGP so created in these experiments rather behave like a strongly coupled liquid. The parameter that decides the material property of such a QGP is its specific viscosity. According to our current understanding about the evolution of the early universe, there were two symmetry breaking processes and therefore two phase transitions, (i) the spontaneous breaking of electroweak symmetry taking place at a few hundred MeV, and (ii) the spontaneous breaking of chiral symmetry of the SU(3) color group at $T < 200$ MeV. For finite quark mass the lattice QCD and common wisdom suggest that at least at small μ_B both should occur at a common T_c. At near-zero net baryon density non-perturbative lattice QCD places this confinement - deconfinement transition at an energy density of about a few GeV/fm^3, and at a critical temperature $T_c \approx 170$ MeV [53–58]. At $\mu_q \approx 0$ the transition is a cross-over at around $T \sim 150 - 170$ MeV, whereas QCD predicts that in a baryon rich environment the transition to deconfinement is of first order. One should therefore expect a QCD critical end point (CEP) where the first order transition line ends up at the cross over. To locate the CEP is of current research interest. At the CEP the first order transition becomes continuous, resulting in long range correlations and fluctuations at all length scales. For a system in between, the above two

limits i.e. (i) $\mu_B = 0$ and high T, and (ii) $T = 0$ and high μ_B, there is a pressure arising from the thermal motion of the particles as well as from the degeneracy of the Fermion gas. The study of the intermediate region of the phase diagram is quite complicated as perturbation theory cannot be applied to the QCD near T_c. Furthermore at finite baryon density the usual lattice approach fails [23, 54, 59]. There exist however, various other effective theories and phenomenological models [8, 60] which form the basis of the QCD phase diagram shown very naively in Figure 1.7.

1.3 QGP signals

One must identify appropriate signals that can detect a QGP state created in high-energy heavy-ion collisions. Formation of QGP is followed by expansion and cooling of the fireball. Below the confining temperature T_c, color neutral hadrons are formed and freeze-out. A hot and dense HG forms the background in this case. The task is to identify the QGP signals from a debris of hundreds, sometimes thousands of particles. This is rather difficult because one requires a precise knowledge of the HG under extreme conditions of temperature and density. The picture for a HG that we employ, either involves an equilibrated statistical system or an ideal, non-interacting system or we consider nuclear collisions as multiple, coherent hadron-hadron collisions etc. We are not sure whether such idealized pictures can describe the ultra-relativistic heavy-ion collisions in a realistic manner. The standard method used in the QGP diagnostics is to compare the prediction of heavy-ion collisions incorporating the presence of QGP with the prediction of models that involves the dynamics of a hot and dense HG. In case we find any anomaly or difference between the two pictures, we can subscribe it to an exotic phenomenon, e.g. QGP formation. In high-energy nuclear collisions we expect multiple scatterings and hence a rapid increase in the entropy followed by a quick thermalization. An important question is whether confinement survives this thermalization or not. In case it does, we have hadrons in the system, if it does not we have a QGP in the fireball. Some of the signatures commonly used to detect the QGP or a QGP-like state are very qualitatively summarized below.

1. J/Ψ **Suppression:** Quarkonia are bound states of heavy quark-antiquark pairs. They are smaller than even the light hadroncs and are much tightly bound. Therefore, they can survive in a QGP even above the deconfinement temperature and melt down only when the color screening radius drops down to the quarkonium size. Since different quarkonium states have different sizes and binding energies, this will lead to a sequential suppression of the quarkonia, first the larger and loosely bound excited states, and then the smaller and tightly bound states [61]. Such patterns can provide a spectral

analysis of the QGP, similar to that obtained for the sun by studying the solar spectra. An alternative explanation for the J/Ψ suppression involves J/Ψ collisions with the hard deconfined partons present in the QGP [62]. A J/Ψ produced somewhere in the fireball has to cross a certain region of hadronic/partonic matter before escaping the collision region, and because it can interact inelastically with particles on its way out, it may be destroyed. A survival probability can be defined as, $\exp(-L/\lambda)$, where L is the distance traveled by the J/Ψ, $\lambda = (n\sigma_{abs})^{-1}$ is the absorption mean free path and n is the particle number density within the fireball medium [63].

As a hard process charm production in nuclear collisions increases with collision energy much faster than that of the light quarks. At sufficiently high energy the produced medium should contain more charm quarks than present in a QGP at chemical equilibrium. If at the hadronization point the charm and anticharm quarks combine statistically to form charmonium states, the combination mechanism should lead to an enhanced J/Ψ production, even if all the direct J/Ψ-s are dissociated [64]. The sequential suppression and statistical regeneration, thus present two opposite patterns. It should be emphasized that statistical recombination would on one hand provide clear evidence for the presence of a thermal medium. On the other, it presupposes a statistical charmonium production mechanism, quite distinct from the hard production that is generally discussed.

2. **Jet Quenching:** In very high-energy collisions, when a parton belonging to a nucleon of one of the incoming nuclei collides with that of the other coming from the opposite direction, high p_t partons are produced. They are commonly referred as jet-partons, they fly off in every possible directions from the collision point, and finally fragment into hadrons emitted in narrow cones. When some of these jet-partons enter a thermalized fireball, they interact with the medium and loose their energies and momenta before hadronization [65]. This loss is commonly known as the jet quenching, and is estimated through a mathematical ratio known as the nuclear modification factor (see Equation (1.33)). If there is no jet quenching then the ratio must be unity for all jet momenta. However, if the ratio tends to be less than unity, it serves as a definite measure of jet suppression in the medium [66–71]. This particular mathematical entity is a suitable candidate for the signature of formation of a themalized medium of deconfined quarks and gluons.

3. **Photon production:** One of the proposed signals of QGP is the direct photon production. The direct photons are defined to be all produced photons, except those coming from hadron decays in the last stage of the collision. There are several processes that can produce the direct photons [72]. The dominant contributions come from the annihilation processes like $q\overline{q} \rightarrow g\gamma$, $q\overline{q} \rightarrow \gamma\gamma$, from the QCD Compton processes

like $qg \rightarrow q\gamma$, $\overline{q}g \rightarrow \overline{q}\gamma$, and from the electromagnetic Bremsstrahlung of quarks, $q \rightarrow q\gamma$. The photon mean free paths are much larger than the transverse size of the region of hot matter created in any nuclear collision, because photons interact only electromagnetically with the medium. As a result, photons with high-energy created in the core of the strongly interacting plasma, can generally pass through the surrounding matter without much interaction, carrying information directly from wherever they are formed. In the hadronic phase the dominant contributions come from processes like $\pi\pi \rightarrow \rho\gamma$, $\pi\rho \rightarrow \pi\gamma$, $\pi\pi \rightarrow \eta\gamma$, $\pi\eta \rightarrow \pi\gamma$ reactions and the $\omega \rightarrow \pi^0\gamma$, $\rho^0 \rightarrow \pi^+\pi^-\gamma$ decays. Thus there is a huge amount of background radiation. For ultra-relativistic nuclear interactions it will be an exceptional thermometer if the thermally produced photon component can be separated from the background. The high-p_t photons can be used to estimate the momentum of the associated parton, allowing a characterization of the in-medium parton energy loss. The prompt photons carry information about the initial state and its possible modifications in nuclei, and should thus be one of the best probes of gluon saturation. The thermal photons emitted from the fireball matter carry information on its temperature. Since quarks and gluons have different momentum distributions in the QGP and hadronic phase, one can get information about a transition to the QGP phase by analyzing the photon spectrum. Hydrodynamic models applied to QGP have shown that the increase in photon number at large p_t is a QGP signal [73].

4. **Lepton pair production:** Production of direct lepton pairs like e^+e^- or $\mu^+\mu^-$ is one of the reliable probes of hot and dense fireball [74]. Leptons interact only electroweakly with the fireball medium and subsequently leave the interphase region without any much interaction carrying information about the properties of the matter at the time when they were produced. Dileptons are mainly produced by thermal $q\bar{q}$ annihilation ($q\bar{q} \rightarrow e^+e^-$ or $q\bar{q} \rightarrow \mu^+\mu^-$) in the QGP phase, and by the decay of ρ, ω and ϕ mesons in the mixed phase. Furthermore, the decays and Bremsstrahlung processes of mesons and baryons after hadronization can produce leptons. ρ meson provides a special opening to observe in-medium modifications of the vector meson properties such as mass and/or width, which may be associated to the chiral symmetry restoration because of a very short lifetime. For ρ meson $\tau = 1.3$ fm/c, as compared to the typical fireball lifetime of $10 - 20$ fm/c at SPS energies. In the analysis of the invariant mass spectrum of the lepton pairs, the primary problem lies in differentiating the contributions coming from different processes. Taking into account of the chiral symmetry restoration, modification of the ρ meson decay channels predicts an increase in the lepton pairs in the intermediate mass region which is supported by experimental results [75].

5. **Charge fluctuations:** Estimation of charge fluctuations would tell us if we have created a system of quarks and gluons [76, 77]). In the QGP phase the unit of charge is $\pm e/3$, while in the hadronic phase the unit of charge is $\pm e$. The net charge of course does not depend on such subtleties, but the fluctuation in the net charge depends on which phase it originates from. Measurement of charge fluctuation is affected by volume fluctuation, which can be avoided if one considers the ratio fluctuations. The task is to find a suitable ratio whose fluctuation is easy to measure and simply related to the net charge fluctuation. An obvious candidate can be the ratio $H = Q/N_{ch}$, where $Q = N_+$ - N_- is the net charge and $N_{ch} = N_+ + N_-$ is the total charge. N_+ and N_- are respectively the number of positively and negatively charged particles. Instead of using H one may as well consider the charge ratio R_{ch}=N_+/N_-. The charged particle multiplicity is directly related to the entropy production. The observable

$$\xi \equiv \langle N_{ch}\rangle\langle \delta R_{ch}^2\rangle = 4\ \langle N_{ch}\rangle\langle \delta H^2\rangle = 4\,\langle \delta Q^2\rangle/\langle N_{ch}\rangle \tag{1.48}$$

provides a measure of the charge fluctuation per unit entropy. The observable differs between a hadronic system and a QGP. For a pion gas $\xi_\pi \approx 4.0$. Relating the final state charged particle multiplicity N_{ch} to the number of primordial quarks and gluons is not simple. One has to use entropy conservation [76] which leads to $\xi_{QGP} \simeq\ 3/4$. Event-by-event fluctuation study of conserved quantities like electrical charge, baryon number, strangeness etc. may allow us to locate the CEP.

6. **Hanbury-Brown-Twiss effect:** Correlation between identical particles or interferometry, provides information about the reaction geometry, and hence gives major information about the spacetime structure of the particle emitting source in AB collisions. The information can be extracted by using the two-particle intensity interferometry technique, also known as the Hanbury-Brown-Twiss (HBT) effect [78, 79]. The method was initially developed to measure the angular size of distant stars [80]. The two-particle correlation arises from the interference of particle wave-functions. This kind of correlation depends on whether the particles are bosons or fermions. The degree of interference depends on the degree of coherence of the particle emitting source(s), which is maximum for a completely incoherent source. The source size increases with event multiplicity and decreases with transverse momentum. If QGP is produced it will hadronize populating the central rapidity region. Following the second law of thermodynamics the volume V and entropy S of the QGP and hadronic phase will be related as $V_{qgp} \times S_{qgp} \leq V_{had} \times S_{had}$. Information regarding the final hadronic phase can therefore be used to understand the nature of the intermediate phase(s).

1.4 Multiparticle production

In any collision involving two elementary objects, be they hadrons, nucleons or nuclei, the interaction cross-section (σ) is of primary importance. In emulsion experiments the cross-section is determined by measuring the interaction mean free path. The theoretical framework of cross-section determination is often given by a geometrical (participant-spectator) or optical model. A good parameterization of the AB interaction cross-section is done by using the Bradt-Peters formula [26],

$$\sigma_{AB} = \pi r_0^2 \left(A^{1/3} + B^{1/3} - \delta \right)^2 \tag{1.49}$$

where r_0 and δ are two parameters determined by fitting the measured cross-sections. Detailed studies on the cross-section measurement showed that δ also depends on the mass number of the colliding nuclei and in the CERN-SPS energy region its variation can be parameterized as,

$$\delta = \delta_0 \left(A^{-1/3} + B^{-1/3} \right)$$

No significant energy dependence has been observed for the nuclear inelastic scattering cross-section. The total inelastic cross-section however, shows variation with energy because of the contribution from Electromagnetic Dissociation (ED) events, which becomes significant at higher energies. In relativistic heavy-ion collisions ED of the projectile nucleus takes place via the exchange of a virtual photon between the projectile and target nuclei. At CERN-SPS energies ($E_{\rm lab} = 200A$ GeV) the maximum energy of the photons that can be exchanged between the interacting nuclei may be as high as $E_\gamma = 4$ GeV. For a low energy photon exchange the nuclei may electromagnetically interact through a dipole (multipole) resonance, causing the target nucleus to excite and then to deexcite by evaporating fragments. On the other hand for a high energy photon they may interact by exciting a Δ (1232) resonance that decays into a nucleon and a pion, either of which can initiate a two-step process of intranuclear cascade accompanied by evaporation tracks [81]. A comprehensive review of multiparticle production in AB collisions at RHIC energies by using thermal and hadronic models can be found in [82]

1.4.1 Multiplicity distribution

It is customary to write down a two body $\rightarrow$ n-particle inclusive reaction as,

$$A \ + \ B \Rightarrow p_1 + p_2 + \cdots + p_n + X$$

where X stands for anything, i.e. all possible particles that are not subjected to observation in a given experiment. In contrast, a reaction like

$$A \ + \ B \Rightarrow p_1 + p_2 + \cdots + p_n$$

where all the final-state particles are detected, is called an exclusive one. A high-energy AB interaction can be represented as,

$$\text{Projectile } (A) \ + \ \text{Target } (B) \ \Rightarrow \ \text{Nuclear fragments} \ + \ \text{Produced particles}$$

In this type of collisions different types of new particles are produced, most of which ($\gtrsim 90\%$) are π-mesons. The number of particles belonging to a particular species in an event is called the multiplicity of that particular species. By measuring the multiplicity one gets an idea about the degrees of freedom released in the collision process. In AB collisions the term multiplicity usually refers to the number of charged hadrons, if not mentioned otherwise. As mentioned before the multiplicity distribution can also be used to determine the impact parameter of the AB collisions. The multiplicity distribution of charged hadrons was found to be well described by the negative binomial distribution (NBD)

$$P_{\rm NBD}(n;\mu,k) = \frac{\Gamma(n+k)}{\Gamma(n+1)\,\Gamma(k)} \, \frac{(\mu/k)^n}{(1+\mu/k)^n} \tag{1.50}$$

for the first time in $p\bar{p}$ collisions [83], and then for other high-energy collisions involving hadrons, leptons, and nuclei. Equation (1.50) uses two free parameters μ and k related respectively to the mean multiplicity as $\mu = \bar{n}$, and its dispersion as $D = \bar{n} + (\bar{n})^2/k$. Sometimes a double-NBD is required to satisfactorily describe the tail of the distribution. The physical interpretation of NBD was given in terms of a clan picture [84]. Several independent clans are produced in the pp collision. Particles belonging to a particular clan have a common history and they are strongly correlated. In high-energy AB collisions the same idea is used to describe the multiplicity distributions in narrow centrality intervals. For a particular centrality class the clan number is given by,

$$N_{\rm clan} = w \times N_{\rm part} \ + \ (1-w) \times N_{\rm coll} \tag{1.51}$$

As mentioned before $N_{\rm part}$ corresponds to soft processes and $N_{\rm coll}$ to hard processes, while w is a weight factor. The charged hadron multiplicity for AB collisions at a given impact parameter is generated by sampling $N_{\rm clan}$ times the pp, or equivalently the NN multiplicity, the latter being generated by NBD. Finally a χ^2 minimization is done by fitting the charged particle multiplicity data obtained from the experiment. The χ^2 minimization gives us the values of w, μ and k, and allows us to connect the experiment with the Glauber model [85].

1.4.2 Pseudorapidity distribution

The (pseudo)rapidity distribution of charged hadrons produced in heavy-ion collisions is an extremely useful global observable that helps us understand several important aspects of multiparticle production. It tells us to what extent the incoming beam energy is utilized to produce new particles. The distributions are single Gaussian shaped when the baryon stopping is significant. For relatively transparent collisions, as is the case in RHIC or LHC experiments, they look like double Gaussian. The distribution is divided into three regions, the projectile fragmentation, the central and the target fragmentation region. At AGS/SPS energies the central region is narrow, and is rich in baryons. On the other hand at top RHIC/LHC energies the central region is wide and almost flat with a small dip at the center. As predicted by the Landau's model the distributions have a functional form like, $dN_{ch}/dy \propto \exp\sqrt{(y_P^2 - y^2)}$, where $y_P = \ln(\sqrt{s_{NN}}/m_p)$ is the projectile rapidity [86]. At higher energies the central (pseudo)rapidity density of charged hadrons $dN_{ch}/d\eta|_{\eta_0}$ becomes higher. We have already seen how in the framework of Bjorken's hydrodynamic model, this central density can be used to determine the initial energy density produced in the AB collisions. For a particular centrality class $dN_{\rm ch}/d\eta|_{\eta_0}$ is also a good measure of the collision centrality. The tails of the distributions are found to be independent of the collision energy, a feature known as longitudinal scaling. If the distributions are plotted as functions of $y' = y - y_P$, they look identical around $y' = 0$. According to the limiting fragmentation hypothesis, the observed (pseudo)rapidity density of particles approaches a limiting value in the fragmentation region even if the colliding energy is increased. Landau's hydrodynamical model predicts that the (pseudo)rapidity spectra of the produced particles should follow a Gaussian distribution [42, 43]. However, fitting a double Gaussian function to the pseudorapidity spectra is motivated by the trend of the data coming from the SPS, RHIC and LHC. The extracted width-parameter is used to study the dynamics of the system. With increase in energy the width of (pseudo)rapidity distribution increases. Using Landau's model this can be related to the longitudinal flow and velocity of sound (c_s) in the fireball medium,

$$\sigma_y^2 = \frac{8}{3}\,\frac{c_s^2}{1 - c_s^4}\,\ln\left(\frac{\sqrt{s_{NN}}}{2m_p}\right)$$

where m_p is the proton mass and σ_y is the width of the (pseudo)rapidity distribution. For an ideal gas $c_s^2 = 1/3$. The central (pseudo)rapidity density of charged hadrons shows a linear-log energy dependence in the SiS100 to RHIC range ($\sqrt{s_{NN}} = 2 - 200$ GeV). A weighted combination of the experimental values of particle yield (central particle density per participant pair) in central AB collisions follows an empirical relation like [87, 88],

$$\frac{2}{N_{\rm part}} \times \left.\frac{dN_{ch}}{d\eta}\right|_{\eta=0} = \alpha + \beta \ln \sqrt{s_{NN}} \tag{1.52}$$

where α and β are fit parameters. Such a behavior seems well justified by the participant-driven picture of the $N_{\rm part}$ scaling of the central density. In addition, as the data show, the process of bulk production is largely characterized by $N_{\rm part}$ or soft scaling, rather than by the number of binary collisions, $N_{\rm coll}$, the latter being attributed to hard scaling. On the other hand the energy dependence of the particle yield in the top RHIC to LHC range can be fitted by a power law,

$$\frac{2}{N_{\rm part}} \times \frac{dN_{ch}}{d\eta}\bigg|_{\eta=0} = \alpha \ (\sqrt{s_{NN}})^{\beta} \tag{1.53}$$

but overestimates the lower energy measurements. The fit parameters α, β are obviously different from the previous equation. The energy dependence of the mean multiplicities, integrated over a finite region of central (pseudo)rapidity, are seen to follow a second-order logarithmic polynomial like [87],

$$\frac{2}{N_{\rm part}} \times N_{ch}\bigg|_{\eta=0} = \alpha + \beta \ \ln(s_{NN}) + \gamma \left[\ln(s_{NN})\right]^2 \tag{1.54}$$

once again with a new set of fit parameters. This trend holds even for relatively low-energies. Such a behavior is expected to be a natural consequence of a combination of the Gaussian shape of the (pseudo)rapidity distribution as predicated in Landau's model, the logarithmic increase of the midrapidity density with the c.m. energy, and the limiting fragmentation. The NN inelastic scattering cross-section increases with energy, which affects the $N_{\rm coll}$ value in AB collisions. As a result the particle yield will have a significant energy and centrality dependence. It is observed that the charged hadron yield at mid-rapidity can be factorized in terms of its energy and centrality dependence in the following way [88],

$$\frac{2}{N_{\rm part}} \times N_{ch}\bigg|_{\eta=0} = f(\sqrt{s}) \times g(N_{\rm part}) \tag{1.55}$$

A fit result to the experimental data provides the following functional forms,

$$\begin{aligned} f(\sqrt{s}) &= \alpha + \beta(\ln s)^2 \\ g(N_{\rm part}) &= 1 + \beta' \, N_{\rm part}^{1/3} \end{aligned} \tag{1.56}$$

1.4.3 Transverse momentum distribution

The hard scattering in nuclear collisions was for the first time reported at CERN ISR [89]. Since this discovery the inclusive p_T measurement has become an important tool in high-energy interactions. An exponential fall of the invariant p_T spectra at low to moderate p_T is a characteristic of a thermalized hadronic system [90]. Any deviation from the exponential

form may therefore be attributed to the partonic structure or some other exotic phenomena [91]. One example of such observation is the suppression of high p_T hadron production in Au+Au collisions at top RHIC energy relative to the pp case at the same energy [90]. The JACEE collaboration, while studying ultra-relativistic cosmic-ray events, observed a rapid increase in the $\langle p_T \rangle$ from its typical range $\langle p_T \rangle \approx 0.34 - 0.4$ GeV/c measured at the collider experiments. For some events the observed value was even ≥ 1 GeV/c, while the energy density of those events was about $2-3$ GeV/fm^3 [92]. According to [93] a sudden increase in the $\langle p_T \rangle$ value could be an indicator of QGP to hadron transition. Although energy densities comparable to the JACEE events have been achieved in the laboratory, no striking change in the p_T spectra has been observed so far [94]. Some results based on hydrodynamical calculations predict only a modest increase in the $\langle p_T \rangle$-value for inclusive charged hadrons, even when the QGP phase is taken into account [95]. A hydrodynamical calculation with strong and electromagnetic decays of resonances upto mass 1.4 GeV [96], cannot predict the SPS data on Pb+Pb interactions at $\sqrt{s} = 17$ GeV [97]. Recently, the transverse momentum spectra of strange hadrons within extensive and nonextensive statistics have been studied over a wide range of collision energy [98]. The hadronic cascade model UrQMD gives much steeper p_T spectra at SPS energies [99], and at RHIC the model prediction given an even steeper p_T spectra. This signifies that the UrQMD is not quite capable to produce enough radial flow. Recently the STAR experiment at RHIC published their beam energy scan results for Au+Au interactions [90]. The p_T spectra for identified hadrons measured by the STAR show a mass ordering, that is the inverse slope of the spectra follow an ordering like $\pi < K < p$. The STAR results can be reproduced by a simple thermal model [100], which indicates a possibility of thermalization of the hadronic matter at RHIC. The p_T spectra can also be used to extract the baryo-chemical potential [90], which enriches our information regarding the QCD phase diagram.

1.4.4 Azimuthal angle distribution

In high-energy heavy-ion collisions the particles produced show a high degree of collective behavior which is termed as flow [101]. Due to a spatial asymmetry present in the overlapping volume of the colliding nuclei, a pressure gradient is generated at an early stage of the collision, that leads to an anisotropic transverse collective flow during the expansion of the hot and dense matter [102]. By characterizing the asymmetric azimuthal distribution of particles (commonly charged hadrons) emitted from non-central collisions, we can quantify the outward pressure. The non-zero Fourier components of the invariant azimuthal distribution

$$E\frac{d^3N}{d^3p} = \frac{1}{2\pi}\frac{d^2N}{p_t dp_t dy}\left(1 + 2\sum_{n=1}^{N} v_n \cos[n(\varphi - \Psi_R)]\right) \tag{1.57}$$

can be used to characterize the collective behavior of the particles. Here Ψ_R is the azimuthal angle of the reaction plane, a plane spanned by the impact parameter and the beam direction. v_1 measures the total amount of in-plane transverse flow. In an AB collision as the participating nucleons try to stop each other, due to a bounce-off effect exerted by the compressed and heated fireball, the spectator nucleons of the impinging nuclei are deflected away from the beam axis. The directed flow of high-p_T particles produced at the very early stage of an AB collision, continues to evolve until the very late stages. Therefore, directed flow can be used to look into the early time thermalization or even into the pre-equilibrium stage of an AB collision. The v_2 coefficient, also called the elliptic flow parameter, originates from the geometrical asymmetry present initially in the almond shaped transverse overlap region of the colliding system. This spatial asymmetry results in an asymmetry in the momentum space, which in turn gets converted to a pressure gradient in the reaction plane, and ultimately to an azimuthal anisotropy in the final state. At high energies the longitudinal dimension of the Lorentz contracted nuclei is negligible in comparison with their transverse dimension. Correspondingly, the time taken by the nuclei to cross each other, becomes small compared to the characteristic time taken by the elliptic flow to develop. The triangular flow parameter v_3 on the other hand originates from the fluctuations of the initial collision geometry. Unlike the elliptic flow, it should not be very sensitive to the centrality of the collision. The triangular flow parameter v_3 has been found to be able to explain the 'near side ridge' and the 'away side shoulder' observed in the two-particle correlations [103]. An investigation based on the viscous hydrodynamics shows that the triangular flow is more sensitive to the QGP viscosity than the elliptic flow [104]. Such type of Fourier decomposition really measures particle emission directly correlated with the orientation of the density gradients as shown by the fact that v_2 for all charged particles at low transverse momenta scales linearly with the eccentricity of the overlap region of the colliding nuclei [105]. In the high-p_t region hadronization occurs through fragmentation, whereas in the medium-p_t region it is modeled by quark recombination or coalescence. The phenomenon of constituent quark number scaling gives experimental support to this model. When scaled by the constituent quark number, the v_2 against E_t curves merge into one universal curve, suggesting that elliptic flow actually develops at the quark level, and hadrons form through combination of constituent quarks.

Bibliography

[1] J. C. Collins and M. J. Perry, Phys. Rev. Lett. 34, 1353 (1975).

[2] E. V. Shuryak, Phys. Rep. 61, 71 (1980).

[3] D. J. Weir, Gravitational Waves from a First Order Phase Transition, https://saoghal.net/slides/brda/, University of Helsinki (2019).

[4] L. P. Csernai and J. I. Kapusta, Phys. Rev. Lett. 69, 737 (1992).

[5] J. Berges and K. Rajagopal, Nucl. Phys. B 538, 215 (1999).

[6] M. A. Stephanov, K. Rajagopal and E. V. Shuryak, Phys. Rev. Lett. 81, 4816 (1998).

[7] Z. Fodor and S. D. Katz, JHEP 0404, 050 (2004).

[8] H. Satz, Extreme States of Matter in Strong Interaction Physics, Lect. Notes in Phys. 841, 1 (2012).

[9] F. Karsch, Lect. Notes Phys. 583, 209 (2002).

[10] F. Karsch, Nucl. Phys. A 698, 199 (2002).

[11] R. S. Bhalerao, CERN-2014-001, pp. 219-239 (2013), arXiv:1404.3294v1.

[12] E. Eichten, K. Gottfried, T. Kinoshita, J. Kogut, K. D. Lane, and T.-M. Yan, Phys. Rev. Lett. 34, 369 (1975).

[13] S. Hands, Contemp. Phys. 42, 209-225 (2001), arXiv:0105022v1.

[14] D. Griffiths, Introduction to Elementary Particles, John Wiley and Sons Inc. (1987).

[15] J. Beringer *et al.* (Particle Data Group), Phys. Rev. D 86, 010001 (2012).

[16] A. Deur, S. J. Brodsky, G. F. de Teramond, Prog. Part. Nuc. Phys. 90, 1 (2016).

[17] D. J. Gross and F. Wilczek, Phys. Rev. Lett. 30, 1343 (1973).

[18] H. D. Politzer, Phys. Rev. Lett. 30, 1346 (1973).

[19] U. Heinz and M. Jacob, arXiv:nucl-th/0002042 (2000).

[20] J. Rafelski, Eur. Phys. Jr. A 51, 114 (2015).

[21] B. Friman, C. Höhne, J. Knoll, S. Leupold, J. Randrup, R. Rapp and P. Senger (Eds.), The CBM Physics Book, Springer (2010).

[22] J. P. Lansberg, Physics of Ultrarelativistic Heavy-ion Collisions, Talk given in the Energy Atlas Workshop, Benasque, Spain (2015).

[23] C. Y. Wong, Introduction to High-Energy Heavy-Ion Collisions, World Scientific (1994).

[24] M. Kliemant, R. Sahoo, T. Schuster and R. Stock, Lect. Notes Phys. 785, 23 (2010), The Physics of the Quark-Gluon Plasma: Introductory Lectures, (Eds.) S. Sarkar, S. Satz and B. Sinha, Springer-Verlag, Berlin, Germany (2010).

[25] https://cerncourier.com/a/participants-and-spectators-at-the-heavy-ion-fireball/.

[26] H. L. Bradt and B. Peters, Phys. Rev. 77, 54 (1950).

[27] P. Shukla, arXiv:nucl-th/0112039v1 (2001).

[28] G. H. Corral, arXiv:1010.3164v1, Lectures given at the 5th CERN-Latin-American School of High-Energy Physics, Recinto Quirama, Colombia, 15 - 28 Mar 2009.

[29] M. L. Miller, K. Reygers, S. J. Sanders, and P. Steinberg, Ann. Rev, Nucl. Part. Sci. 57, 205 (2007).

[30] D. Kharzeev and M. Nardi, Phys. Lett. B 507, 121 (2001).

[31] X.-N. Wang and M. Gyulassy, Phys. Rev. Lett. 86, 3496 (2001).

[32] N. Herrmann *et al.*, Ann. Rev. Nucl. Part. Sci. 49, 581 (1999).

[33] J. Adams *et al.* (STAR Collaboration), Nucl. Phys. A 757, 102 (2005).

[34] J. Letessier and J. Rafelski, Hadrons and Quark-Gluon Plasma, Cambridge University Press, Cambridge (2004).

[35] R. Hagedorn, Nuovo Cim. Suppl. 3, 147 (1965).

[36] R. Hagedorn and J. Rafelski, Phys. Lett. B 97, 136 (1980).

[37] R. Hagedorn, Z. Phys. C 17, 265 (1983).

[38] E. Fermi, Prog. Theo. Phys. 5, 570 (1950).

[39] A. Chodos, B. L. Jaffe, K. Johnson, C. B. Thorn and V. F Weisskopf, Phys. Rev. D 9, 3471 (1974); A. Chodos, B. L. Jaffe, K. Johnson and C. B. Thorn, Phys. Rev. D 1O, 2599 (1974).

[40] R. Vogt, Ultrarelativistic Heavy-Ion Collisions, Elsevier, Amsterdam, The Netherlands (2007).

[41] D. Evans, QCD and the Quark-Gluon Plasma, Talk given in the Summaer School, Queen's University, Belfast, UK (2017).

[42] L. D. Landau, Izv. Akad. Nauk. Ser. Fiz. 17, 51 (1953).

[43] S. Z. Belensky and L. D. Landau, Usp. Fiz. Nauk. 56, 309 (1955).

[44] I. M. Khalatnikov, J. Exp. Theor. Phys. 26, 529 (1954).

[45] P. Carruthers and M. Duong-Van, Phys. Rev. D. 28, 130 (1983).

[46] S. Pokorski and L. Van Hove, Acta. Phys. Pol. B 5, 229 (1974).

[47] L. Van Hove and S. Pokoroski, Nucl. Phys. B 86, 243 (1975).

[48] J. D. Bjorken, Phys. Rev. D 27, 140 (1983).

[49] K. Yagi, T. Hatsuda and Y. Miake, Quark-Gluon Plasma, From Big Bang to Little Bang (Cambridge University Press, Cambridge, 2005).

[50] P. Kolb and U. Heinz, Quark-Gluon Plasma 3, (Eds.) R. C. Hwa and X. N. Wang, World Scientific, Singapore (2003).

[51] M. Stephanov, Prog. Theo. Phys. Suppl. 153, 139 (2004).

[52] M. Gazdzicki, M. Gorenstein and P. Seyboth, Act. Phys. Pol. B 42(2), 307 (2011).

[53] L. Susskind, Phys. Rev. D 20, 2610 (1979).

[54] J. Kuti, J. Polónyi and K. Szlachányi, Phys. Lett. B 98, 199 (1981).

[55] J. Engels, F. Karsch, I. Montvay and H. Satz, Phys. Lett. B 101, 89 (1981).

[56] F. R. Brown *et al.*, Phys. Rev. Lett. 65, 2491 (1990).

[57] F. Karsch, Nucl. Phys. A 590, 367 (1995).

[58] R. Stock, hep-ph/9901415 24.

[59] L. D. McLerran *et al.*, Phys. Lett. B 98, 195 (1981); Phys. Rev. D 24, 450 (1981).

[60] A. Ayala *et al.*, Nucl. Phys. B 897, 77 (2015).

[61] T. Matsui and H. Satz, Phys. Lett. B 178, 416 (1986).

[62] D. Kharzeev and H. Satz, Phys. Lett. B 334, 155 (1994).

[63] D. Kharzeev, C. Lourenco, M. Nardi and H. Satz, Z. Phys. C 74, 307 (1997).

[64] P. Braun-Munzinger and J. Stachel, Nucl. Phys. A 690, 119 (2001);
R. L. Thews, M. Schroedter and J. Rafelski, Phys. Rev. C 63, 054905 (2001).

[65] J. D. Bjorken, Fermilab-Pub-82/59-THY, Batavia (1982).

[66] M. Gyulassy and M. Plümer, Phys. Lett. B 243, 432 (1990).

[67] M. H. Thoma, Quark Gluon Plasma 2, (Ed.) R. C. Hwa, p.51, (World Scientific, 1995).

[68] R. Baier, Nucl. Phys. A 715, 209c (2003).

[69] R. Karabowicz (BRAHMS Collaboration), Nucl. Phys. A 774, 477 (2006).

[70] A. Grelli (ALICE Collaboration), Nucl. Phys. A 904, 635c (2013).

[71] M. B. Tonjes (CMS Collaboration), Nucl. Phys. A 904, 713c (2013).

[72] J. Kapusta, P. Lichard and D. Seibert, Phys. Rev. D 44, 2774 (1991).

[73] P. Huovinene and P. V. Ruuskanen, Ann. Rev. Nucl. Part. Sc. 56, 163 (2006).

[74] E. L. Feinberg, Nuovo Cimento A 34, 391 (1976).

[75] I. Tserruya, Nucl. Phys. A 681, 133c (2001).

[76] S. Jeon and V. Koch, Phys. Rev. Lett. 85, 2076 (2000).

[77] M. Asakawa, U. Heinz and B. Müller, Phys. Rev. Lett. 85, 2072 (2000).

[78] G. Goldhaber *et al.*, Phys. Rev. 120, 300 (1960).

[79] U. A. Wiedemann and U. W. Heinz, Phys. Rept. 319, 145 (1999).

[80] R. Hanbury-Brown and R. Q. Twiss, Nature 178, 1046 (1956).

[81] G. Singh, K. Sengupta and P. L. Jain, Phys. Rev. C 41, 999 (1990).

[82] A. Tawfik and E. Abbas, Phys. Part. Nucl. Lett. 12, 521 (2015); F. Karsch, K. Redlich and A. Tawfik, Eur. Phys. J. C 29, 549 (2003); A. Tawfik, Phys. Rev. D 71 054502 (2005); F. Karsch, K. Redlich and A. Tawfik, Phys. Lett. B 571, 67 (2003).

[83] G.J. Alner *et al.* (UA5 Collaboration), Phys. Lett. B 160, 193 (1985); *ibid* 160, 199 (1985).

[84] A. Giovannini and L. Van Hove, Z. Phys. C 30, 391 (1986).

[85] R. Sahoo *et al.*, Adv. High Energy Phys. 2015, 612390 (2015).

[86] L. D. Landau, Multiple production of particles under collision of rapid particles, in Collected Papers of L. D. Landau, Ed. D. Ter-Haar, pp. 569–585, Pergamon Press, Oxford, UK, 1965.

[87] E. K. G. Sarkisyan and A. S. Sakharov, Eur. Phys. J. C 70, 533 (2010).

[88] B. Alver *et al.* (PHOBOS Collaboration), Phys. Rev. C 83, 024913 (2011).

[89] B. Alper *et al.*, Phys. Lett B 44, 52 (1973);
M. Banner *et al.*, Phys. Lett. B 44, 537 (1973).

[90] L. Adamczyk *et al.* (STAR Collaboration), Phys. Rev. C 96, 044904 (2017).

[91] J. Schukraft, International Workshop on Quark Gluon Plasma Signatures, 127-143, Cern Report number: CERN-PPE-91-04.

[92] T. H. Burnett *et al.*, Phys. Rev. Lett. 57, 3249 (1986).

[93] L. Van Hove, Phys. Lett. B 118, 138 (1982);
E. V. Shuryak and O. V. Zirhov, Phys. Lett. B 89, 253 (1980).

[94] J. Schukraft, Proc. 19th Int. Symp. on Multiparticle Dynamics, Arles 1988 (World Scientific, 1988).

[95] M. Kataja *et al.*, Phys. Rev. D 34, 2755 (1986);
J. P. Blaizot and J. Y. Ollitrault, Nucl. Phys. A 458, 745 (1986);
X. N. Wang and R. C. Hwa, Phys. Rev. D 35, 3409 (1987).

[96] P. Huovinen *et al.*, Phys. Lett. 503, 58 (2001).

[97] H. Appelshäuser *et al.* (NA49 Collaboration), Phys. Rev. Lett. 82, 2471 (1999).

[98] A. N. Tawfik, Adv. High Eng. Phys. 2019, 4604608 (2019); H. Yassin, E. R. Abo Elyazeed and A. N. Tawfik, Phys. Scr. 95, 075305 (2020).

[99] M. J. Bleicher *et al.*, Phys. Rev. C 62, 024904 (2000).

[100] W. Florkowski and W. Broniowski, Nucl. Phys. A 715, 875 (2003).

[101] H. A. Gustafsson *et al.*, Phys. Rev. Lett. 52, 1590 (1984).

[102] J.-Y. Ollitrault, Phys. Rev. D 46, 229 (1992).

[103] B. Alver and G. Roland, Phys. Rev. C 81, 054905 (2010); *ibid.* 82, 039903 (2010).

[104] B. Schenke *et al.*, Phys. Rev. Lett. 106, 042301 (2011).

[105] C. Adler *et al.* (STAR Collaboration), Phys. Rev. Lett. 87, 182301 (2001).